

# Chapter 8

## Biomechanics and Biotribology of UHMWPE Artificial Hip Joints



Yongchang Gao and Zhong-Min Jin

**Abstract** Well function of hip joints ensures daily movements such as walking, standing, climbing, or lifting. However, joint diseases such as osteoarthritis, rheumatoid arthritis, and trauma often require the natural bearings to be replaced by artificial ones. John Charnley pioneered the first metal-on-polyethylene artificial hip joints in the 1960s, when he articulated a femoral head against the ultrahigh molecular weight polyethylene (UHMWPE) liner. Although ceramic-on-ceramic and metal-on-metal artificial hip joints have been widely used in clinic, the UHMWPE hip implants are most prevailing with great success. Currently, over one million patients accept total hip replacement around the world every year, and the demand remains increasing with the accelerated aging population. However, unlike natural synovial hip joints with excellent elasto-hydrodynamic lubrication, artificial hip joints overall experience boundary lubrication or mixed lubrication. Under such lubrication conditions, direct contact between femoral head and acetabular liner is inevitable and finally generates extensive micro-wear debris. Then bioreaction of soft tissues rendered by UHMWPE wear particles occurs, which eventually leads to aseptic loosening of hip implants in the long term. In the past decades, much research enhancing wear resistance of the UHMWPE hip implants has been done by polymer scientists, biomedical engineers, orthopedic surgeons, and manufacturers. This chapter aims to review the latest research on wear performance of UHMWPE artificial hip joints from both biomechanics and biotribology.

---

Y. Gao

School of Construction Machinery, Chang'an University, Xi'an, Shaanxi, China

Z.-M. Jin (✉)

Tribology Research Institute, School of Mechanical Engineering, Southwest Jiaotong University, Chengdu, Sichuan, China

State Key Laboratory of Manufacturing System Engineering, School of Mechanical Engineering, Xi'an Jiaotong University, Xi'an, Shaanxi, China

Institute of Medical and Biological Engineering, School of Mechanical Engineering, University of Leeds, Leeds, UK

e-mail: [zmjin@mail.xjtu.edu.cn](mailto:zmjin@mail.xjtu.edu.cn)

© Springer Science+Business Media Singapore 2019

J. Fu et al. (eds.), *UHMWPE Biomaterials for Joint Implants*, Springer Series in Biomaterials Science and Engineering 13,  
[https://doi.org/10.1007/978-981-13-6924-7\\_8](https://doi.org/10.1007/978-981-13-6924-7_8)

241

**Keywords** UHMWPE · Hip joint implants · Lubrication · Wear · Biomechanics · Biotribology · Hip joint simulator · Wear debris

## 8.1 Introduction

### 8.1.1 UHMWPE Artificial Hip Joints

Natural synovial hip joints are one of the most important joints for human to achieve all kinds of movements. It is expected to function well in the human body for a lifetime while transmitting large dynamic loads and yet accommodating a wide range of movements. However, diseases such as osteoarthritis, rheumatoid arthritis, and trauma often require these natural bearings to be replaced by artificial hip implants [1]. Total joint replacement has proved to be the most successful surgical treatment for hip joint diseases for more than 50 years [2].

At present, more than one million hip joint replacements are carried out every year all over the world [3, 4]. Up to now, three kinds of material combinations are introduced and widely used in clinic for artificial hip joints: metal/ceramic femoral head vs polymer (UHMWPE) cup, ceramic femoral head vs ceramic cup, and metal femoral head vs metal cup [5–7]. However, the majority of these devices utilize a material combination of ultrahigh molecular weight polyethylene (UHMWPE) as the acetabular cup articulating against either a ceramic (alumina) or a metallic (stainless steel, cobalt-based alloy) femoral head (Fig. 8.1). This mostly applied

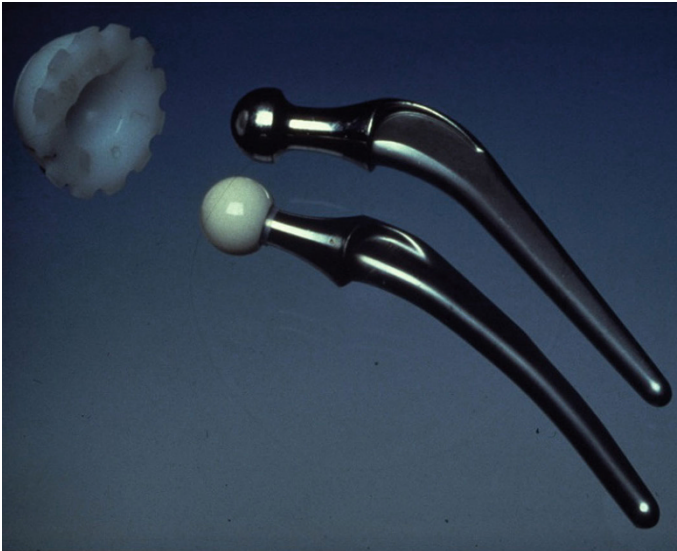


**Fig. 8.1** A typical Charnley hip prosthesis consisting of an UHMWPE acetabular cup against either a metallic (stainless steel) or a ceramic (alumina) femoral head

combination, however, encountered with severe wear problems, which will be described in Sect. 8.2. This section concentrates on UHMWPE artificial hip joints.

### ***8.1.2 Complications After Total Hip Replacement***

The patient who has adopted total hip replacement (THR) could fully or almost relieve from serious pain and recover daily movement. The hip implants can last 15 years in about 90% of those who received them [5]. However, there are still some complications with total hip replacement because of the huge demands. After a few weeks of total hip replacement, the most common and serious complication are blood clots in the legs and infection of operation side [8], respectively. These short-term complications can be reduced with improvements in sterile technique and medical treatment in surgery.

The most important long-term complication is aseptic loosening, which occurs over time and can cause problems with the function of the hip prosthesis. What's worse, the loosened hip implants need to be revised. Dislocation is another long-term common complication for THR [9, 10], which ranks only second to aseptic loosening. Berry et al. [9] investigated the dislocation rate of THR and observed a gradual increase over time.

### ***8.1.3 Relationship Between Aseptic Loosening and Wear for THR***

Hip implants experience daily movements such as walking, running, climbing, lifting, and even standing and sitting. The implant takes large forces and a range of motions [11, 12]. Generally, patients with hip implants take about one million steps per year in average [13], and younger patients move more than this average level. On the one hand, such motions and starting/stopping lead to both collision and relative sliding between the femoral head and the cup. On the other hand, in vivo hip implants mainly undergo mixed lubrication [14], which results in a poor separation of the articulating surfaces by the lubricant. Thus, the wear of hip implants is inevitable to generate wear debris, as has been verified both in vivo and in vitro. The majority of wear debris ranges from 0.1  $\mu\text{m}$  to 1  $\mu\text{m}$  [15, 16]. These UHMWPE microparticles released from the articulating interface enter the periprosthetic tissues and are taken up by macrophages. The macrophages release a range of mediators of inflammation including cytokines in an attempt to eliminate these bio-inert particles. Meanwhile, such mediators have osteolytic effects and cause the gradual loss of bones surrounding the hip implants, which eventually lead to aseptic loosening of the prosthesis.

The aseptic loosening is the result of long-term accumulation of hip implant wear. Thus, most prostheses could still function well in several years. For conventional UHMWPE hip implants, 90% of them could last 15 years after surgery [17]. However, the wear performance of UHMWPE hip implants plays a major role in the long-term success of the medical devices. Much research work in this field is focusing on wear and wear debris-induced osteolysis in currently used artificial hip joints, by using both experimental and theoretical tools to conduct tribological studies on contact mechanics, friction, lubrication, and wear.

### ***8.1.4 Relationship Between Biomechanics and Wear for THR***

Wear of hip implants resulted from contact and relative motion between the femoral head and acetabular cup is described in Sect. 8.3. Hence, the contact mechanics [18] and kinematics [19] need to be carefully investigated during the research of hip implant wear. Biomechanics covers the study of the structure and function of biological systems such as humans, animals, plants, organs, fungi, and cells by using the methods of mechanics. Both contact mechanics and kinematics of hip implants belong to biomechanics. Specially, biomechanics of hip implants mainly refer to the mechanical properties of soft tissue and bones and their preoperative and postoperative movements [20]. More details about biomechanics of hip implants are described in Sect. 8.2.1.

## **8.2 Biomechanics of Artificial Hip Joints**

### ***8.2.1 Introduction***

The main objectives of THR are to reduce pain, improve range of motion, and restore joint function of patients [21–24]. Recovery of muscle strength and mechanical performance as well as motions are the basis to achieve these aims of THR. The following three paragraphs will give a brief introduction to biomechanics of artificial hip joints before detailed research is presented.

The hip implant supports quite large loads generated by muscle activity pulling the prosthesis, the weight of the limbs and trunk. Therefore, it is of great importance to recover the strength of muscles surrounding the hip implant. The postoperative strength of most muscles shows a gradual increase in the first year of surgery and then keeps stable over time. However, the muscle's strength could not recover to the level of the healthy side. It is difficult to measure the hip contact force related to muscle strength. The most common way to obtain hip contact force is to use musculoskeletal system [25, 26], which is often used to estimate the internal joint loading, joint kinematics, and muscle forces. Different musculoskeletal multibody

dynamic models have been introduced to predict both hip contact force and motions by using different models, which will be further introduced in the latter sections.

Contact mechanics is a study of load transfer between two contacting solids. The main parameters determined from contact mechanics analysis include contact area and stresses. Contact stresses are generally related to structural failure and fatigue-related wear mechanisms. A large contact area is required to produce a low contact stress under a given load. However, if the contact area is too large, the contact may be extended to the equatorial region and the edge of the cup, not only leading to stress concentrations, limiting the normal movement of the hip joints, but also blocking the lubricant entry and causing lubricant starvation and depletion. In addition to the tribological studies at the bearing surfaces, contact mechanics can be used to simulate the implantation of the prosthetic components (e.g., press fitting) to examine the stresses in the bone and the deformation of the prosthetic components. Much research on contact stresses and contact area has been done and will be introduced in detail in the latter sections.

Kinematics is the study of motion of bodies without referencing to mass or force. In the hip, the geometry of the ball and socket prevents any translation but allows rotation during all kinds of human movements [27]. The relative rotations in all three planes make large sliding distance, which is directly proportional to wear of the prosthesis. The magnitude of sliding distance may be different under different movements and differ in the same movement because of individual characteristics such as walking speed, stride length, etc. What's more, the range of motion is related to actions of muscles, which also influences the relative sliding. The corresponding studies will be presented in the latter sections.

## **8.2.2 Musculoskeletal Multibody Dynamic Simulation**

### **8.2.2.1 Musculoskeletal Modeling Based on Force-Dependent Kinematics**

It is important to understand the performance of muscles after THR because of their influences on both hip contact force and range of hip joint motions as described in Sect. 8.2.1. Currently, the common way to determine hip contact force and range of hip joint motions is musculoskeletal multibody dynamic analysis. Different models of the human musculoskeletal system have been developed over the past decades [28–30] to determine the hip contact force and motions. The majority of musculoskeletal multibody dynamic modeling has been driven by the commercial musculoskeletal modeling system. Hip implants were simplified as a hinge to fulfill relative rotations without considering microseparation state of the hip joint center (HJC) of the femoral head and geometries or material properties [31].

Based on previous musculoskeletal multibody dynamic modeling, Zhang et al. [32] recently introduced a force-dependent kinematics (FDK) approach that considers both the position and the geometry of the femoral head of the hip joint to

simultaneously predict hip contact force and hip joint translation. In this study, a typical hip implant was directly implanted into the left lower limb to replace disabled natural hip joint, and material properties were also taken into account in the model.

The contact force predicted by this method changed over gait cycle and reached the maximum value of about three times body weight. The predicted results of hip contact force agreed with experimental data.

### 8.2.2.2 Effect of Surgical Position on Hip Contact Force

Artificial hip joint is expected to be fixed into the anatomic position to obtain the biggest range of motions for the patient, which is mainly determined by the hip implant center position. For most patients, it is easy to implant the prosthesis into the anatomic position. However, for persons whose hip joint is congenital defect such as developmental dysplasia of the hip, it is rather hard to reposition the hip implant into the anatomic position. Using the FDK method, Zhang et al. investigated the influence of hip implant position on contact forces under both walking and stair climbing.

According to clinic observations, the deviation distance of hip joint center from its anatomic position should not exceed 15 mm. In these studies, the hip implant was set in the maximum deviation distance of 15 mm in six directions. The results of the hip contact force (HCF) under different hip implant centers when the patient walks are shown in Fig. 8.2. The hip contact force in anterior–posterior direction increased if the prosthesis center position deviated 15 mm from the standard position in the lateral, inferior, and posterior directions. In contrast, the hip contact force would decrease under same conditions in the medial, superior, and anterior directions. The variation trend of hip contact force in both lateral–medial direction and superior–inferior direction under different prosthesis positions was in accordance with that in anterior–posterior direction. Furthermore, the hip contact force deviated remarkably increased due to the deviation from the anatomic position (Table 8.1).

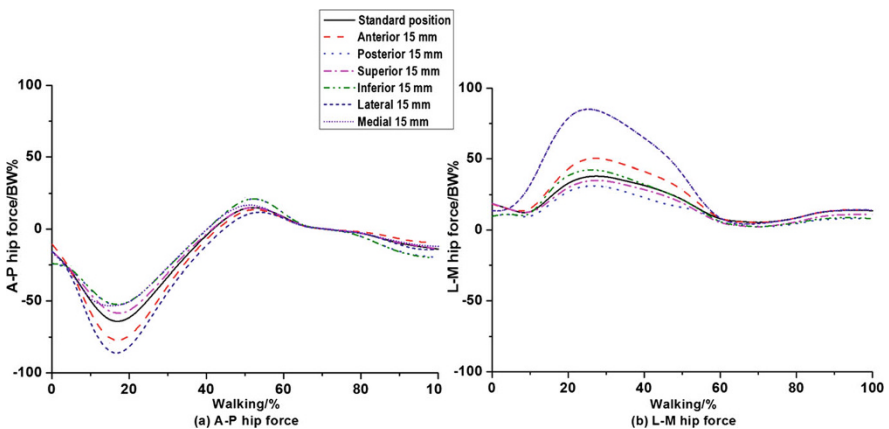


Fig. 8.2 The predicted HCF under different hip joint centers

**Table 8.1** Increasing of the maximum hip contact force when the prosthesis deviated 15 mm from the anatomic position during walking

Unit/ %	Anterior 15 mm	Posterior 15 mm	Superior 15 mm	Inferior 15 mm	Lateral 15 mm	Medial 15 mm
A-P	-17.96	20.86	-8.45	16.59	35.62	-17.71
L-M	-18.38	34.12	-7.75	11.79	125.2	-47.69
S-I	-11.62	16.99	-4.35	3.91	17.39	-14.07

**Table 8.2** Increasing of the maximum hip contact force when the prosthesis deviated 15 mm from the anatomic position during squatting

Unit/ %	Anterior 15 mm	Posterior 15 mm	Superior 15 mm	Inferior 15 mm	Lateral 15 mm	Medial 15 mm
A-P	0.34	-4.81	3.77	-25.72	-17.06	3.04
L-M	5.47	-8.44	4.43	-5.72	-6.38	9.53
S-I	-9.40	6.23	3.23	-12.00	10.93	-19.30

The hip implant force is also influenced if the prosthesis deviates from the anatomic position under squatting movement. The results are shown in Table 8.2. It can be also concluded that the hip implant center would apparently influence the hip contact force.

Therefore, the hip contact force would be apparently influenced by positioning of the hip implant in surgery for both walking and squatting movements. This should be carefully considered in surgery, and the hip implant is prospected to be fixed into the anatomic position.

### 8.2.2.3 Effect of Surgical Approach on Hip Contact Force

For different patients, different surgical approaches may be used during the process of THR. Up to now, posterior approach, lateral approach, and anterior approach are widely used in clinic. For different approaches, the damage of muscles is different. Taking the posterior approach as an example, the gluteus maximus is damaged, but the function of the abductor is kept well. Thus, the hip implant could possess a large range of motions. Zhang et al. used the FDK method to study the influence of surgical approaches on hip contact force.

In this study, all muscle's forces that would be damaged totally or partially under different surgical approaches were multiplied by a damage coefficient (Table 8.3). During walking, the effect of surgical approach on the maximum hip contact force is shown in Table 8.4. It reveals that the maximum hip implant forces of anterior approach and superior approach are obviously different from the normal hip contact force. Using these two kinds of surgical approaches would lead to sharp decrease in the lateral-medial direction but slight increase in the superior-interior direction for the maximum hip contact force. However, the lateral approach had little influence on the hip contact force comparing to the other two surgical approaches.

**Table 8.3** Damage coefficient of muscles under different surgical approaches

Muscles name	Lateral approach	Posterior approach	Anterior approach
Gluteus medius anterior (6)	0.6	0.6	0.8
Gluteus medius posterior (6)	0.6	0.6	0.8
Gluteus minimus anterior (1)	0.6	0.6	0.5
Gluteus minimus medial (1)	0.6	0.6	0.5
Gluteus minimus posterior (1)	0.6	0.6	0.5
Gluteus maximus (12)	1	0.6	1
The tensor fascia lata muscle (2)	0.6	1	1

**Table 8.4** Effect of surgical approach on the maximum hip contact force during walking

Unit/%	Different surgical approaches			
	Anterior approach	Posterior approach	Lateral approach	
	Dev. of Max F	Dev. of Max F	Dev. of Max F	Dev. of Max F
A-P	Heel strike	-7.22	-10.46	-9.98
		±1.56	±2.19	±3.18
	Toe off	+24.91	+24.19	-19.88
		±9.27	±8.73	±6.25
S-I (swing)		+4.04	+4.04	-0.64
		±1.30	±0.39	±0.25
L-M (swing)		-38.47	-44.82	-22.53
		±2.84	±0.84	±1.06

**Table 8.5** Effect of surgical approach on the maximum hip contact force during squatting

Unit/%	Anterior approach	Posterior approach	Lateral approach
A-P	-0.61	1.84	-0.6
L-M	-6.84	0.11	-2.76
S-I	-2.63	1.01	-1.11

The effects of surgical approach on the maximum hip contact force during squatting are shown in Table 8.5. The maximum hip contact force only slightly changed for all three surgical approaches during squatting in comparison with that during walking.

In summary, different surgical approaches would affect hip contact force during walking, and the lateral approach may have much less influence on the hip contact force. Therefore, it is better to consider this factor when choosing surgical approaches.

### 8.2.3 Investigation of Contact Mechanics

As mentioned above, contact pressure and contact area are very important for hip implants. It is preferred to test both contact pressure and contact area in vivo or



in vitro, which has been done in previous studies [33–35]. However, experiments are expensive and time-consuming, which are not suitable for parameterized design of hip implants. Therefore, the numerical method becomes a most appropriate alternative method to predict contact pressure and contact area. To date, the finite element method is the most common numerical method [36, 37]. The related research will be presented in details in the following sections.

Relative sliding, as well as contact, between the femoral head and the acetabular cup is needed to be determined for hip implants. The analytical method, Euler method, has been introduced to calculate accumulated sliding distance of hip implant under different movements. In the latest study, a dynamic finite element method has been developed to predict sliding distance. These studies will be described in the later sections.

What's more, the dynamic finite element method was used to investigate both contact mechanics and relative sliding of the dual mobility hip implant. This will also be fully introduced in the next sections.

### 8.2.3.1 Computational Prediction of Contact Pressure

During the process of finite element modeling, simplified model is generally used to represent artificial hip. Typical finite element model consists of pelvic bone, bone cement, UHMWPE cup, and femoral head, as done by Hua et al. [38] (Fig. 8.3). This model is comprised of an UHMWPE cup, a stainless femoral head, a pelvic bone, and a bone cement. The dimensions were accordance with real implants. The bone cement fixed both pelvic bone and UHMWPE cup together, contact pairs was set between the UHMWPE cup and the stainless femoral head. All parts were meshed using proper element type and size: the femoral head was treated as rigid body

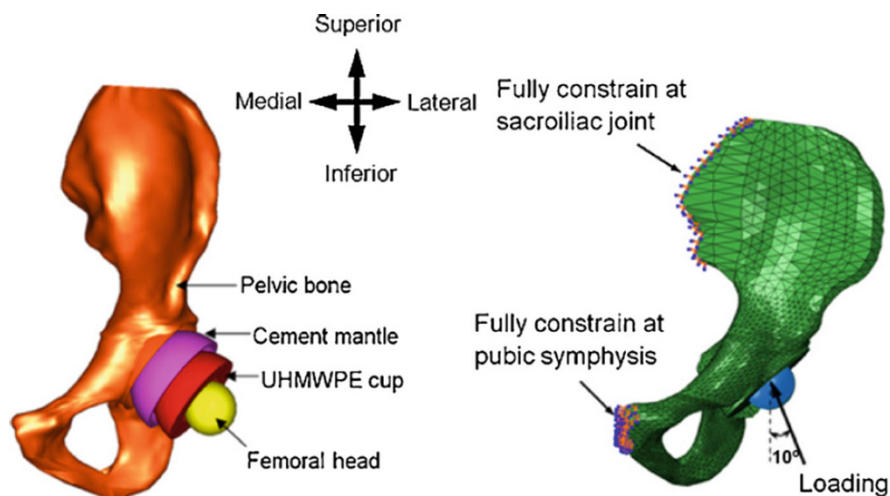


**Fig. 8.3** The geometry (left) and boundary conditions (right) of the hip joint model. (Reprinted from Ref. [38], Copyright 2012, with permission from Elsevier)

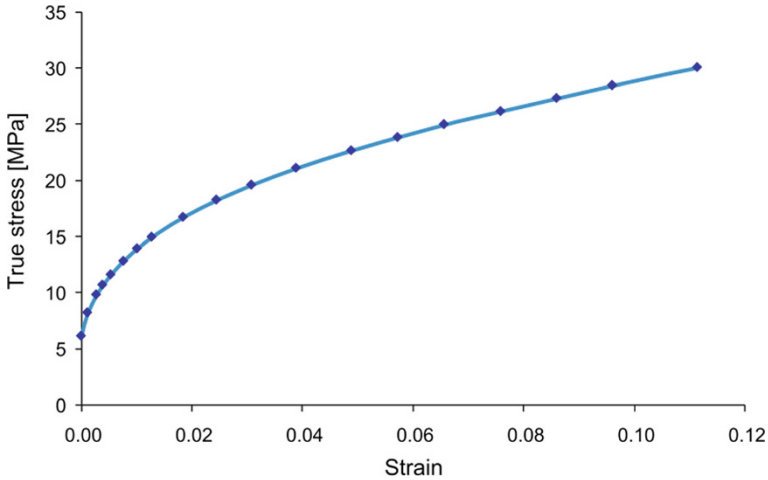


**Fig. 8.4** The plastic stress–strain relation for UHMWPE. (Reprinted from Ref. [38], Copyright 2012, with permission from Elsevier)

because its Young’s modulus was about two orders of magnitude higher than other parts. According to practical restraints, two regions of pelvic bone were fully constrained as shown by the finite element model. A contact force of 2500 N was applied at the femoral head center and with the direction of  $10^\circ$  medially.

The UHMWPE was modeled as nonlinear elastic–plastic based on the plastic stress–strain constitutive relationship (Fig. 8.4). The plastic stress–strain data were taken from Liu [39] for a similar polyethylene material. The other material properties used in this study are given in Table 8.6. Then performing finite element contact statics analysis, both contact pressure and contact area could be predicted.

Using this static finite element method, contact pressure and contact area of hip implants could be predicted. The following several paragraphs show some applications of this method for conventional hip implants.

The *in vivo* results show that the orientation of the acetabular cup was important for hip implant. When an artificial hip joint is implanted into a patient, the orientation of UHMWPE cup is carefully determined because both higher inclination and anteversion angles will lead to poor contact mechanics and severe wear [40–42]. The suggested safe inclination angle is below  $55^\circ$ . The first application using the static finite element method was to investigate the contact mechanics of UHMWPE hip implant under adverse edge loading.

**Table 8.6** Material properties used in study of Hua et al.

Component	Materials	Young’s modulus (GPa)	Poisson’s ratio
UHMWPE cup	UHMWPE	0.85	0.4
Bone cement	PMMA	2.5	0.254
Cortical shell	Cortical bone	17	0.3
Cancellous bone	Cancellous bone	0.8	0.2

Reprinted from Ref. [38], Copyright 2012, with permission from Elsevier

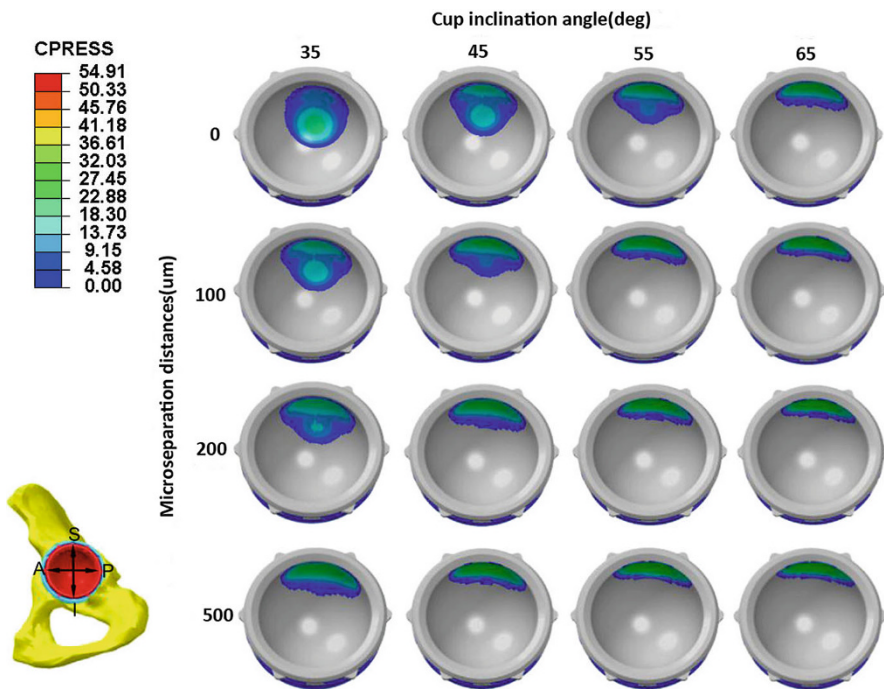


**Fig. 8.5** The distribution of contact pressure (MPa) on the frontside articulating surface as a function of cup inclination angles and microseparation distances [36]

Recently, Hua et al. investigated the contact mechanics of modular metal-on-polyethylene THR under adverse edge loading conditions [36]. Different cup inclination angles coupled with different microseparations, contact pressure, and contact zone (contact area) of UHMWPE cup inner surface were shown in Fig. 8.5. The contact pressure increased with inclination angles and microseparation distance, but the contact zone decreased at the same time. Furthermore, edge contact occurred under high inclination angle and big microseparation distance. Edge contact and higher contact pressure are harmful for both stability and wear performance of artificial hip joints. The predicted result agreed with the clinical observation that a high inclination angle is harmful for the conventional artificial hip joints. Similar results were also reported by Wang et al. [37], who investigated the effects of both inclination and anteversion angles on the contact pressure.

In addition, wear volume and depth directly depend on contact mechanics; the static finite element method has been widely used during computational simulation of wear process of artificial hip joints. Kang et al. [43] and Liu et al. [44] have calculated contact pressure of UHMWPE cup as input of wear calculation of artificial hip joints. Contact pressure varied with different gait cycles and overall decreased with increasing gait cycles, but it nearly did not vary after the first

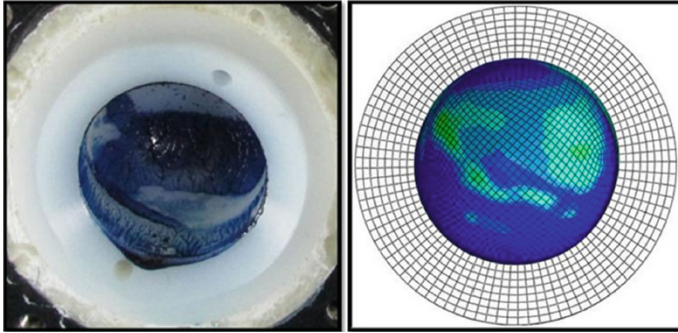


**Fig. 8.6** Comparison of contact area between the finite element model and compression test for one sample of custom-coated hip implant after 5 Mc (million cycles) simulator testing (12.6% cycle, loading 3000 N). (Reprinted from Ref. [45], Copyright 2015, with permission from Elsevier)

10 million gait cycles. This agrees with the fact that the contact pressure will decrease with the increasing contact area.

The contact mechanics of UHMWPE cup after different walking gait cycles has been investigated [45]. The worn surfaces of the cups under different stages of hip simulator testing were reconstructed and were applied to the simulation. The contact areas predicted by finite element method and observed in experiments are compared in Fig. 8.6. It is revealed that contact zone tested in experiment and predicted by static finite element method are consistent. Besides, the results of contact pressure at different walking gait cycles are shown in Fig. 8.7. The results reveal that the contact pressure of UHMWPE cup after wear became much higher than that of unworn (the maximum value at 4 Mc was about 2.5 times than that of unworn). The finding of variation of contact pressure by this study is different from the result by Kang et al.

### 8.2.3.2 Computational Prediction of Sliding Distance

Wear is expected to be proportional to the sliding distance. However, it is hard to determine the sliding distance of implants by experiments. Therefore, it is usually predicted using numerical method, including the Euler method developed by Saikko et al. [46] and Kang et al. [43]. The details of this method are described in the following paragraphs.

When calculating the accumulated sliding distance between the femoral head and the acetabular cup, the hip implant could be simplified to a ball-in-socket model (Fig. 8.8a, b). The transformed simplified spherical coordinates were built at the center of the head, and the spherical coordinates were  $(R_1, \theta, \phi)$ . A separate moving coordinate system,  $x', y', z'$ , was placed at the center of the head and assumed to be fixed relative to the head and to coincide with the center of the cup. Three rotation motions of flexion–extension (FE), abduction–adduction (AA), and internal–external rotation (IER) were assumed to move around the moving axes  $z', x', y'$ ,

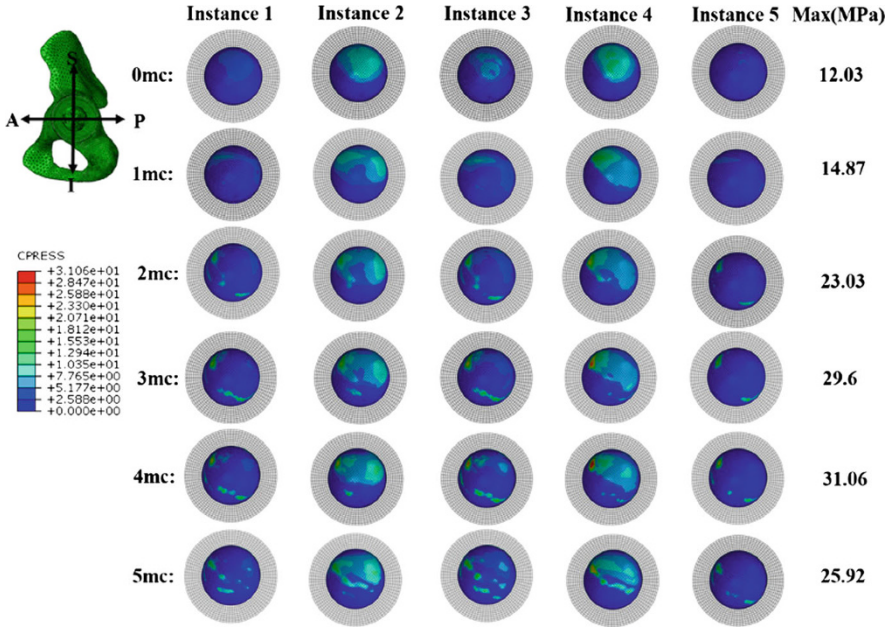


**Fig. 8.7** Contour plot for the contact pressure of the articulating surfaces in realistic model at a series of testing points (0–5 Mc). (Reprinted from Ref. [45], Copyright 2015, with permission from Elsevier)

respectively. The corresponding motion data under walking have been reported by Johnston and Smidt [47]. The hip joint rotated following the Euler sequence of FE→AA→IER, which was used in the computation of sliding distance.

Given that  $\theta$  and  $\phi$  are the spherical coordinates of any point on the head at instant  $i$  in the  $x, y, z$  coordinate system (Fig. 8.8b), the position vector  $\{P_i\}$  for this point is expressed as

$$\{P_i(\theta, \phi)\} = \begin{Bmatrix} R_1 \sin \theta \cos \phi \\ R_1 \sin \theta \sin \phi \\ R_1 \cos \theta \end{Bmatrix} \quad (8.1)$$

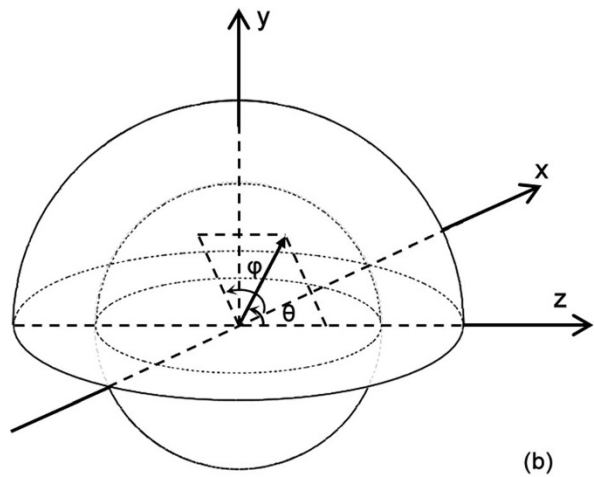
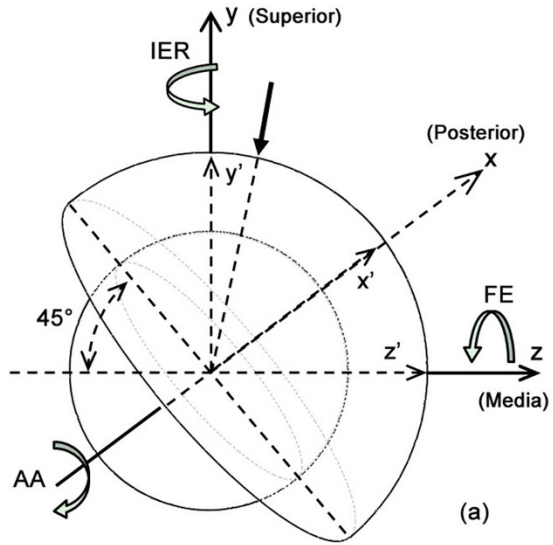
where  $R_1$  is the radius of the head.

As mapped onto the  $x, y, z$  coordinates system (Fig. 8.8a),  $\{P_i(\theta, \phi)\}$  is rewritten as a new position vector  $\{Q_i(\theta, \phi)\}$  according to

$$\{Q_i(\theta, \phi)\} = \begin{bmatrix} \cos \kappa & -\sin \kappa & 0 \\ \sin \kappa & \cos \kappa & 0 \\ 0 & 0 & 1 \end{bmatrix} \begin{bmatrix} 1 & 0 & 0 \\ 0 & \cos \lambda & -\sin \lambda \\ 0 & \sin \lambda & \cos \lambda \end{bmatrix} \times \{P_i(\theta, \phi)\} \quad (8.2)$$

where  $\kappa$  and  $\lambda$  are the anteversion and inclination angles of the cup. The anteversion angle generally varies between  $15^\circ$  and  $20^\circ$  and is fixed as  $0^\circ$  in the present study.

**Fig. 8.8** (a) Ball-in-socket geometry in the anatomical spherical coordinate axes; (b) transformed simplified spherical coordinates



Assuming  $\{Q_i(\theta, \phi)\}$  as the preceding position vector, the new position vector  $\{Q_{i+1}(\theta, \phi)\}$  after one set of rotations at instant  $i+1$  is expressed as

$$\{Q_{i+1}(\theta, \phi)\} = (R_{z'x'y'})_i \{Q_i(\theta, \phi)\} \tag{8.3}$$

where  $(R_{z'x'y'})_i$  is the relative rotation matrix for the rotation sequence FE→AA→IER. Assuming  $\alpha_i$ ,  $\beta_i$ , and  $\gamma_i$  as the rotation angles corresponding to FE, AA, and IER, respectively,  $R_{z'x'y'}$  was given by Craig [39] as

$$(R_{z,x'y'})_i = \begin{bmatrix} -\sin \alpha_i \sin \beta_i \sin \gamma_i + \cos \alpha_i \cos \gamma_i & -\sin \alpha_i \cos \beta_i & \sin \alpha_i \sin \beta_i \cos \gamma_i + \cos \alpha_i \sin \gamma_i \\ \cos \alpha_i \sin \beta_i \sin \gamma_i + \sin \alpha_i \cos \gamma_i & \cos \alpha_i \cos \beta_i & -\cos \alpha_i \sin \beta_i \cos \gamma_i + \sin \alpha_i \sin \gamma_i \\ -\cos \beta_i \sin \gamma_i & \sin \beta & \cos \beta \cos \gamma_i \end{bmatrix} \tag{8.4}$$

The accumulated sliding distance  $\Delta S_j(\theta, \phi, t)$  was calculated as

$$\Delta S_j(\theta, \phi, t) = |\{Q_{i+1}(\theta, \phi) - Q_i(\theta, \phi)\}| \tag{8.5}$$

All accumulated sliding distance could be calculated by combining all above formats. This is so-called numerical Euler method.

Kang et al. has computed the maximum accumulated sliding distance of UHMWPE cup under normal walking gait. The predicted sliding distance by Kang et al. agreed well with that by Calonius and Saikko.

Besides, the Euler method is also used to predict the sliding trace of artificial hip joints, as has been done by Saikko et al. [46] (Fig. 8.9). It can be seen that the sliding trace of most points on femoral head was oval. The results predicted by numerical Euler method generally agreed with the experimental results of the zone. The Euler method is appropriate and convenient to predict sliding distance and trace of conventional hip implant because of the single articulation for this prosthesis.

However, for dual mobility hip implant consisting of two articulations, this method is not suitable any more. To solve this problem, a dynamic finite element method was developed by Gao et al. [47]. This method could be performed as follows.

In this study, both conventional and dual mobility hip implants were modeled using the dynamic finite element method, as shown in Figs. 8.10 and 8.11,

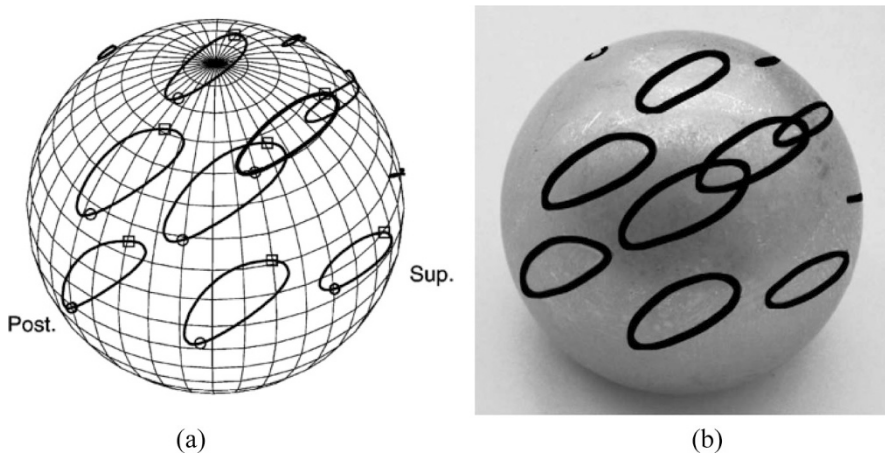
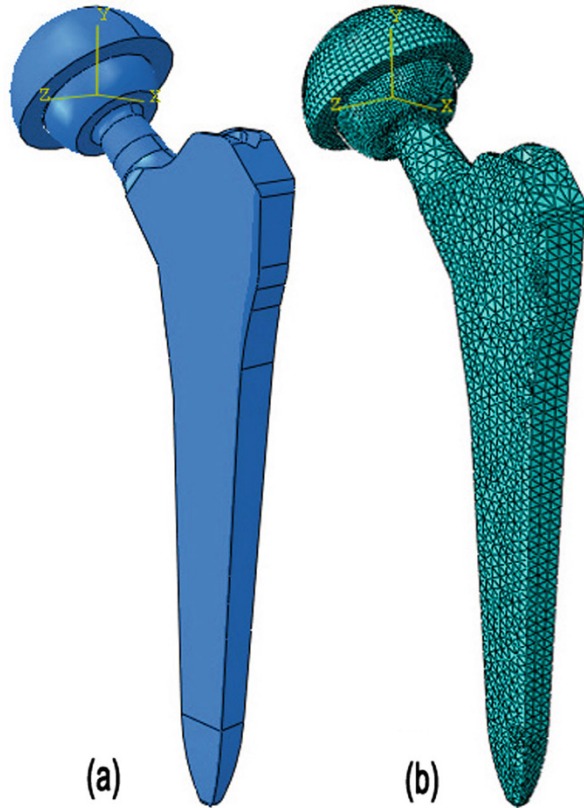


**Fig. 8.9** Comparison of sliding distance of femoral head between (a) numerical results and (b) experimental data by Saikko et al. (Reprinted from Ref. [46], Copyright 2015, with permission from Elsevier)

**Fig. 8.10** (a) CAD and (b) FE models of conventional artificial hip joint using dynamic finite element method



respectively. The conventional hip implant was comprised of UHMWPE cup, CoCr alloy femoral head, and Ti alloy stem; the dual mobility hip implant was comprised of metal back shell, UHMWPE liner, CoCr alloy head, and Ti alloy stem. For both hip implants, the diameter of femoral head was 28 mm. The entire stem was used for both hip implants. UHMWPE was also modeled as nonlinear elastic–plastic material as Hua et al. [38] has done, but other materials were linear elastic. The detailed material parameters for dual mobility hip implant are shown in Table 8.7.

For conventional hip implant, there is only one contacting interface between the femoral head and the cup inner surface. In contrast, two contacting interfaces were modeled for dual mobility hip implant, one between the femoral head and the liner inner surface and the other between the liner outer surface and the back shell inner surface. For these two types of hip implants, all components including contacting surface were meshed by eight-node structured hexahedron elements, while stem was meshed using coarse four-node tetrahedron elements. The UHMWPE cup outer surface was fully constrained for conventional hip implant, but that of the back shell was fixed for dual mobility hip implant.

Both three-dimensional forces and three rotation motions were applied at the center of the femoral head including flexion–extension (FE), abduction–adduction



**Fig. 8.11** (a) CAD and (b) FE models of dual mobility hip implant using dynamic finite element method

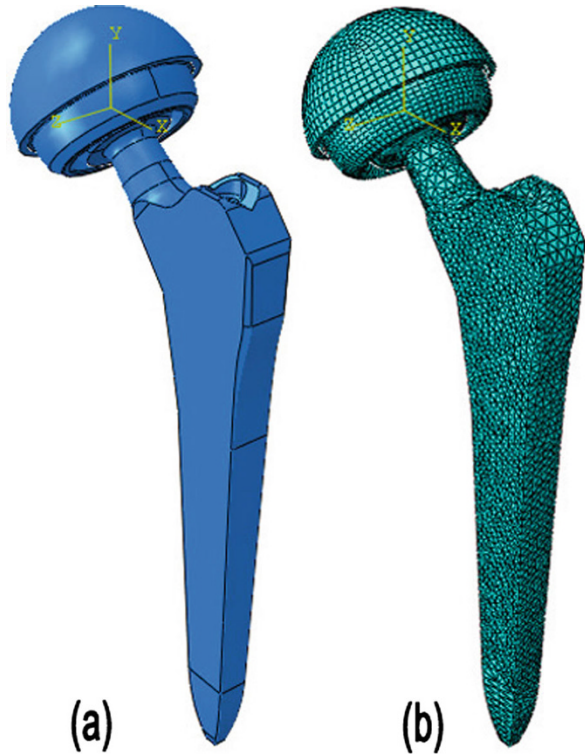


**Table 8.7** Material parameters of the dual mobility hip implant

Materials	Density ( $\text{g/mm}^3$ )	Elastic modulus (GPa)	Poisson's ratio	Yield strength (MPa)
CoCr alloy	7.61	217	0.30	\
UHMWPE	0.932	1	0.45	\
Ti alloy	4.52	110	0.3	23.56

(AA), and internal–external rotation (IER). Forces could be directly applied, but rotation motions could not be used directly. Kang et al. used FE, AA, and IER to describe a typical walking gait. At any instant of a walking gait cycle, FE, AA, and IER refer to the rotation angles from the initial position to the current position. However, during a continuous dynamic process, the stem and femoral only could rotate to a new position from last position rather than from initial position. Therefore, a method was introduced to convert the initial FE, AA, and IER data to a new data so as to simulate continuous dynamic rotations. This method can be used to calculate all incremental rotation vectors between any two adjacent instants of a gait cycle.

Then the method to calculate incremental rotation vector between two adjacent instants was developed. The original FE, AA, and IER angles at a time instant were represented through the Euler rotation angles to enable the stem to rotate continuously from the beginning position to a new position. A moving coordinate system

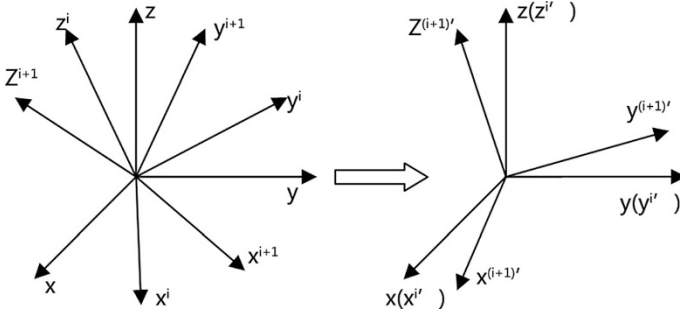


**Fig. 8.12** Incremental rotation vectors calculation by inverse Euler rotation

XYZ was fixed too and located at the center of the femoral head. This moving coordinate system was rotated with the head during a gait cycle, and its initial orientation was in accordance with the fixed coordinate system in Sect. 8.2.1. The Euler rotation started from the FE around the X-axis, followed by the AA and the IER along with Y-axis and Z-axis of the moving coordinate system, respectively [43]. Incremental rotation vectors were therefore calculated, according to the static movement wave forms. The movement wave forms in Sect. 8.2.1 were divided into  $N$  instants. For arbitrary two adjacent instants  $i$  and  $i+1$ , both Euler rotation matrices  $R_i$  and  $R_{i+1}$  were calculated according to Saiko and Calonius [46], and then the incremental rotation vector between these two instants was obtained from the known  $R_i$  and  $R_{i+1}$  [48]. Then inverse Euler rotation  $R_i^{-1}$  was applied to both  $R_i$  and  $R_{i+1}$ , and the incremental rotation vector between  $R_i$  and  $R_{i+1}$  was converted to a new incremental rotation vector corresponding to the fixed coordinate systems. In this way, all incremental rotation vectors corresponding to the fixed coordinate system (Fig. 8.12) were calculated, which could be used to continuous dynamic process [47].

Then, the sliding distance of any position could be calculated by performing the dynamic finite element method.

The predicted sliding distance of the UHMWPE acetabular cup of the conventional hip implant during one walking gait cycle using this method is shown in Figs. 8.13 and 8.14. Sliding distance increased with the gait cycle and reached the

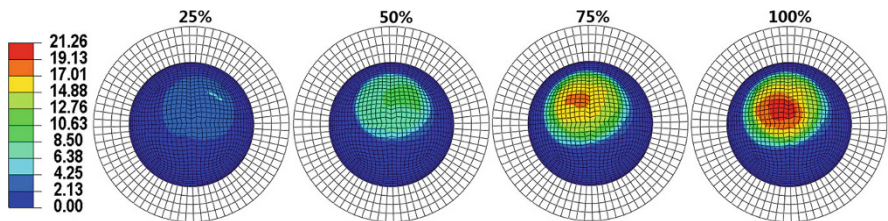
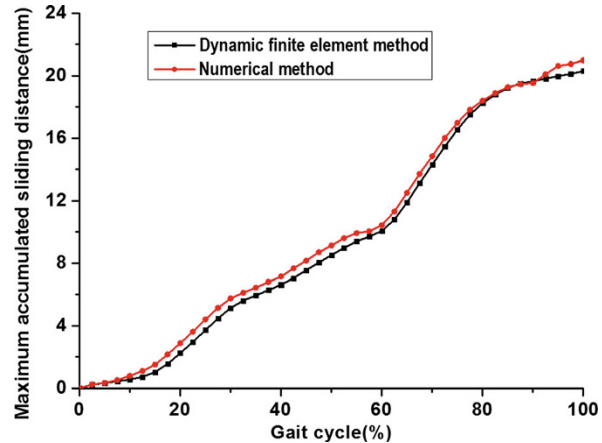


**Fig. 8.13** Contours of the cup inner accumulated sliding distance (mm) at different percentages of the gait cycle for the conventional artificial hip joint model predicted by the dynamic finite element method under a fixed element size of 1.5 mm

**Fig. 8.14** Comparison of the maximum accumulated sliding distance of the cup as a function of the gait cycle for the conventional artificial hip model using different methods



maximum value at the end of gait cycle. The maximum value predicted at each instant was highly consistent with the numerical Euler method. This implies that the dynamic finite element method could be used to calculate sliding distance of conventional artificial hip joints.

### 8.2.3.3 Contact Mechanics of Dual Mobility Hip Implants

As mentioned in Sect. 8.1.2, dislocation is another common long-term complication for artificial hip joint. However, conventional hip implants could not prevent dislocation effectively. Dual mobility hip implant has been introduced by Bousquet in the 1970s [49] and has proved successful in preventing dislocation [50, 51]. For this kind of hip implant, the intermediate UHMWPE liner is not fixed onto the metal cup any more, and thus it could rotate with femoral head under some extreme condition. It is important to understand the biomechanics performance of this kind of implant. The following paragraphs present some research on its biomechanics.

Using the dynamic finite element method, Gao et al. investigated contact mechanics of dual mobility hip implant under different frictions [52]. The influence of friction on contact mechanics for dual mobility hip implant is shown in Figs. 8.15, 8.16, 8.17, and 8.18. For different friction coefficient ratios of dual mobility hip implant, (1) contact pressure and contact area varied with applied loads. However, contact zone was obviously different with a friction coefficient ratio of 1 comparing to that with a friction of coefficient ratio of 1.6. Only relative sliding occurred for inner articulation if friction coefficient ratio was 1, but outer relative sliding happened when friction coefficient ratio increased to 1.6; (2) for different coefficient ratios, the maximum contact area at liner outer surface was evidently higher than that of inner surface, which finally led to contrasting results for the maximum contact pressure of these two surfaces.

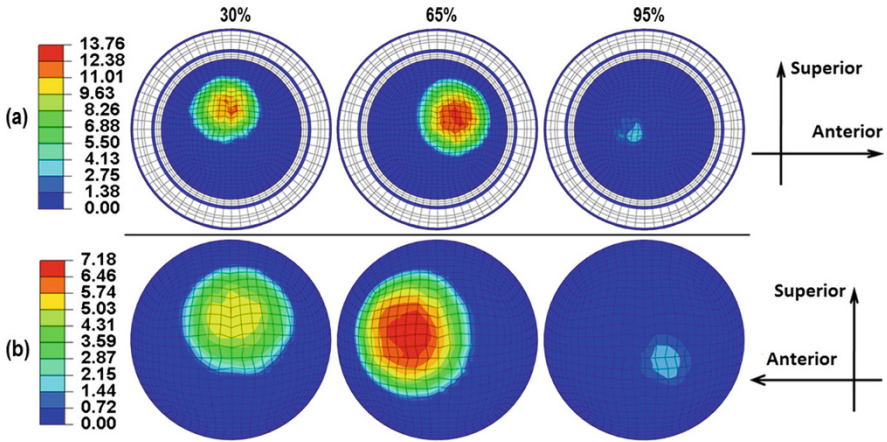


**Fig. 8.15** Contours of the liner contact pressure under a friction coefficient ratio of 1 during different walking instants: **(a)** inner contact pressure (MPa), **(b)** outer contact pressure (MPa)

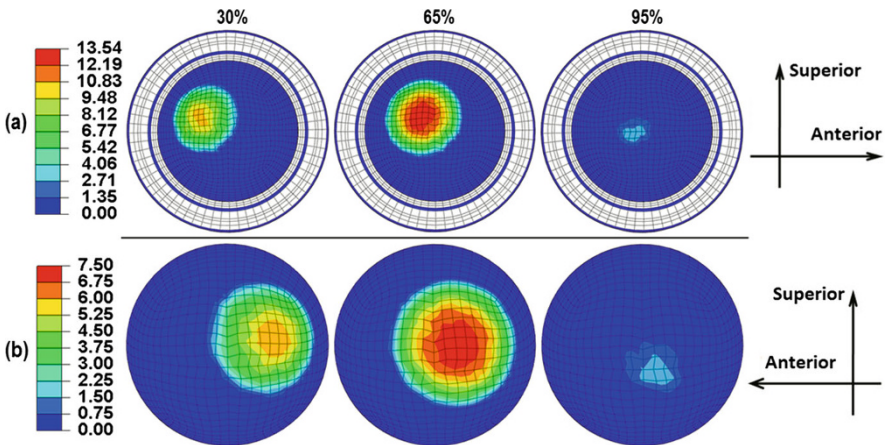


**Fig. 8.16** Contours of the liner contact pressure under a friction coefficient ratio of 1.6 during different walking instants: **(a)** inner contact pressure (MPa), **(b)** outer contact pressure (MPa)

The results of accumulated sliding distance with different friction coefficients are shown in Figs. 8.19 and 8.20. It is concluded that the liner kept static when the ratio of friction coefficient was 1 or 1.23. However, outer relative sliding occurred when the ratio of friction coefficients between two articulations (inner vs outer) increased to 1.6 for dual mobility hip implant. Comparing the maximum sliding distance of the liner outer and inner surface under different ratio of friction coefficient, the outer maximum value was much larger than the inner maximum value. What's more, the liner outer surface possesses a larger contact area than the inner surface when the liner rotated under high ratio of friction coefficient. This means that, if the relative sliding happens for the liner outer surface owing to friction coefficient, it will lead to

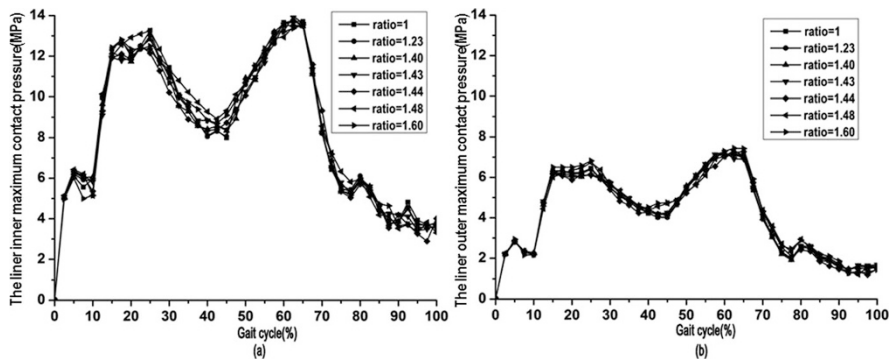


**Fig. 8.17** Maximum contact pressure of the liner as a function of the gait cycle under different friction coefficient ratios of the inner to the outer articulation: (a) inner maximum contact pressure and (b) outer maximum contact pressure

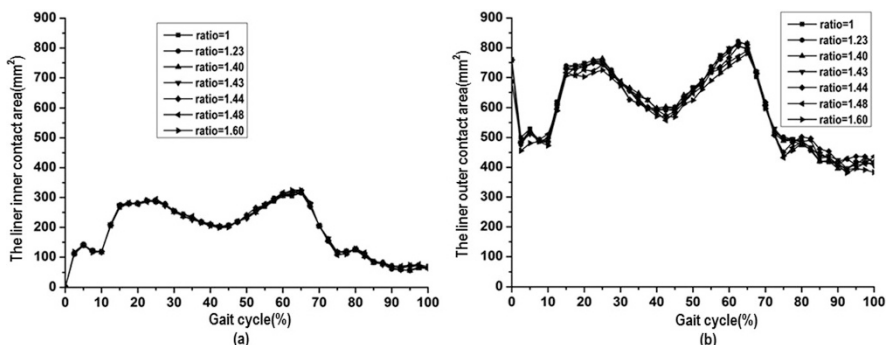


**Fig. 8.18** Contact area of the liner as a function of the gait cycle under different friction coefficient ratios of the inner to the outer articulation: (a) inner contact area and (b) outer contact area

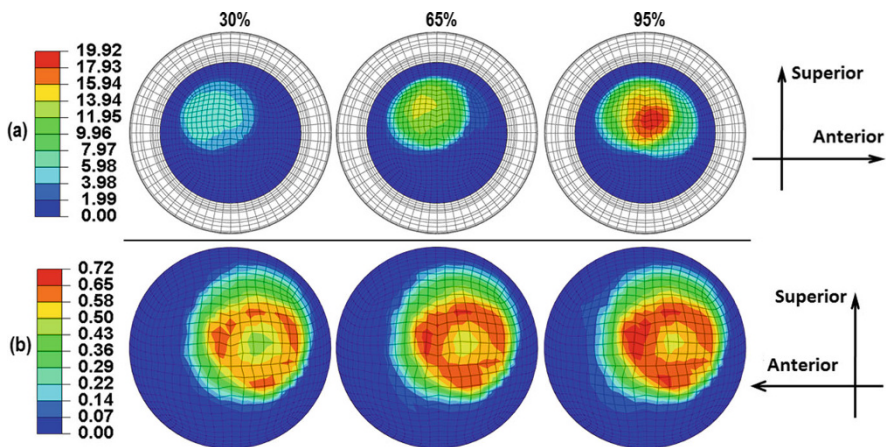


**Fig. 8.19** Contours of the liner accumulated sliding distance under a friction coefficient ratio of 1 during different walking instants: (a) inner accumulated sliding distance (mm) and (b) outer accumulated sliding distance (mm)

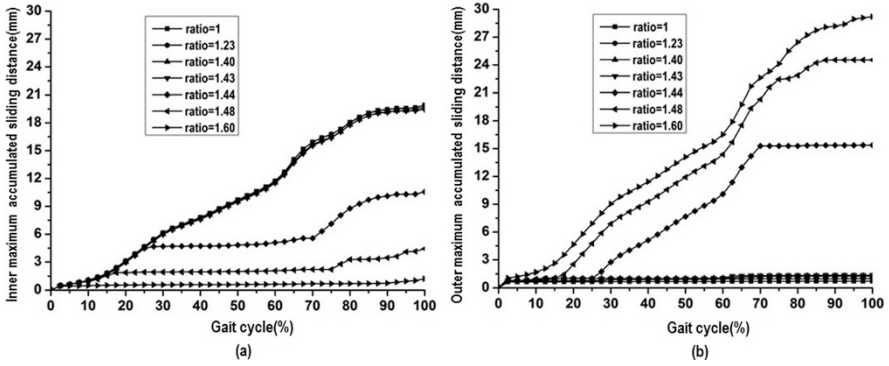


**Fig. 8.20** Maximum accumulated sliding distance of the liner as a function of the gait cycle under different friction coefficient ratios of the inner to the outer articulation: (a) inner maximum accumulated sliding distance and (b) outer maximum accumulated sliding distance

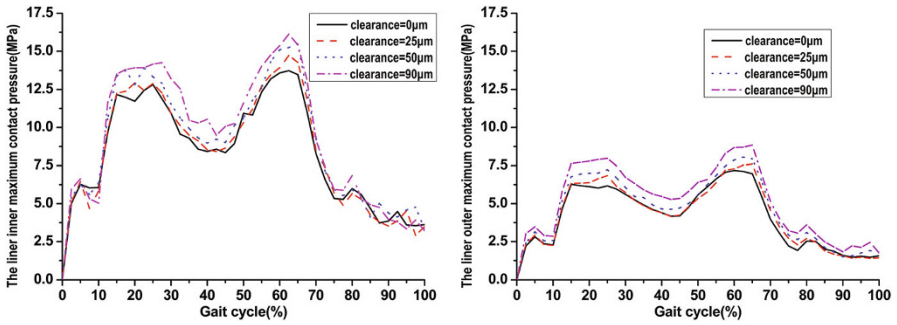


**Fig. 8.21** Maximum contact pressure the liner as a function of the gait cycle under different initial clearances of the outer articulation and a fixed friction coefficient ratio of 1.40: (a) inner maximum contact pressure and (b) outer maximum contact pressure

more wear volume because wear volume is proportional to sliding distance and contact area. The liner outer wear loss of the retrieved dual mobility hip implants from patients is larger than that of the inner side, which could be explained by the rotation of the liner.

Different clearances will influence both the maximum contact pressure and contact area for conventional artificial hip joint according to previous studies. The clearance may also affect the contact mechanics of dual mobility hip implant. In a study by Gao et al., different initial clearances from 0 to 90 μm were set between liner outer surface and back shell inner surface under a constant ratio of friction coefficient of 1.4. The results of the maximum contact pressure and contact area of both surfaces of the liner are shown in Figs. 8.21 and 8.22. The maximum contact pressure of both surface of the liner was slightly increased with clearance increasing. In contrast, the influence of clearance on contact area of liner outer surface was significant. The outer contact area of the liner sharply decreased with the increasing

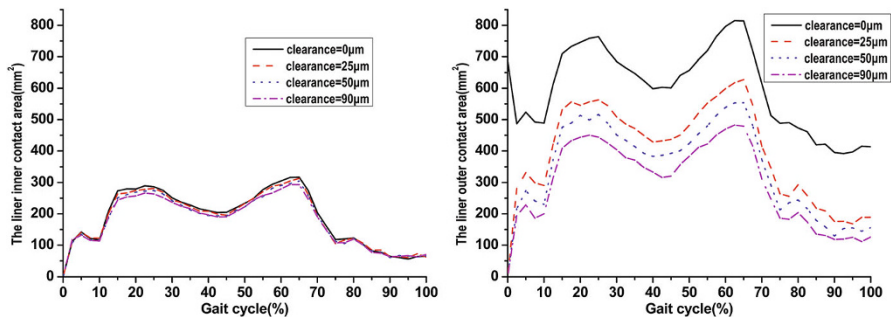


**Fig. 8.22** Contact area of the liner as a function of the gait cycle under different initial clearances of the outer articulation and a fixed friction coefficient ratio of 1.40: (a) inner contact area and (b) outer contact area

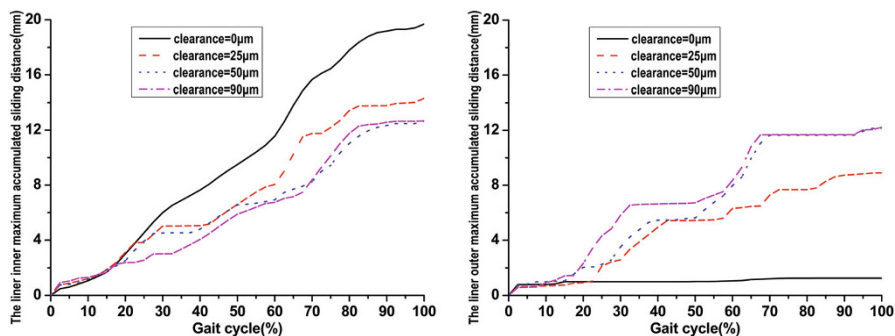


**Fig. 8.23** Maximum accumulated sliding distance of the liner as a function of the gait cycle under different initial clearances of the outer articulation and a fixed friction coefficient ratio of 1.40. (a) Inner maximum accumulated sliding distance. (b) Outer maximum accumulated sliding distance

clearance, but the inner contact area almost remained the same. With different initial interferences between liner outer surface and back shell inner surface, both contact pressure and contact area were different. It may suggest that a tiny clearance could be designed for outer articulation of dual mobility hip implant to decrease the contact area without affecting other performances of contact mechanics.

The maximum sliding distances of the liner inner and outer surfaces under different clearances are shown in Fig. 8.23. It is apparent that the liner kept static when the clearance was zero, but it started to gradually rotate with the head with the increasing clearance. It means that, if the ratio of friction coefficient is slightly lower than the critical value, the clearance of the outer articulation would be helpful for the outer relative movement for the dual mobility hip implant. However, if the friction coefficients were the same at both articulations, increasing outer surface clearance could not lead to the outer movement for dual mobility hip implant.

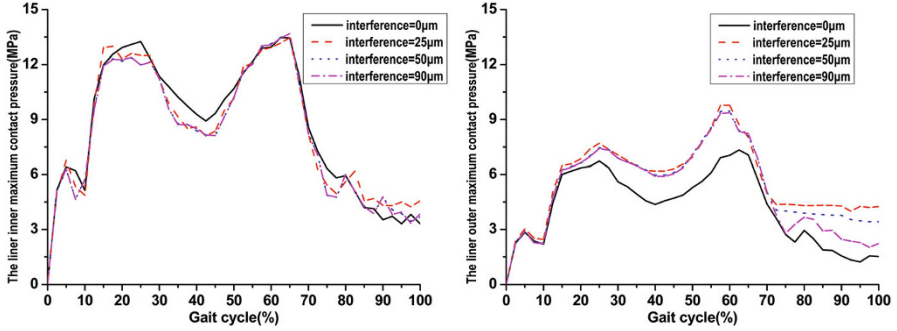


**Fig. 8.24** Maximum contact pressure the liner as a function of the gait cycle under different initial interferences of the outer articulation and a fixed friction coefficient ratio of 1.48: (a) inner maximum contact pressure and (b) outer maximum contact pressure

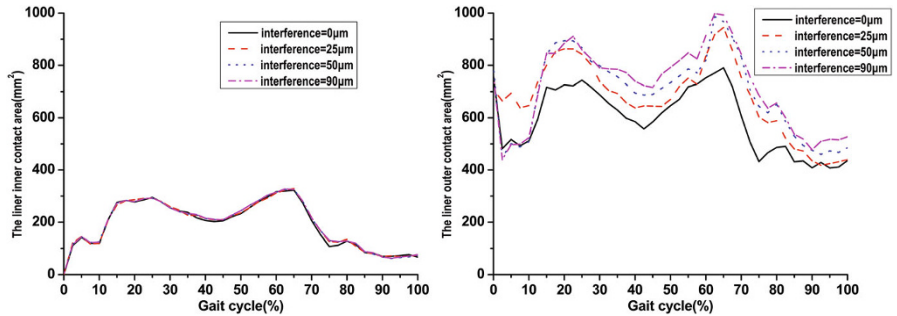


**Fig. 8.25** Contact area of the liner as a function of the gait cycle under different initial interferences of the outer articulation and a fixed friction coefficient ratio of 1.48: (a) inner contact area and (b) outer contact area

Similarly, different interferences from 0 to 90 μm were set between the liner and the back shell to investigate its effect on contact mechanics and kinematics for dual mobility hip implant. The results of contact pressure and contact area under different initial interferences are shown in Figs. 8.24 and 8.25. The results are different from those with different initial clearances for dual mobility hip implant. Initial interferences between the liner outer surface and the back shell inner surface did not affect the liner inner maximum contact pressure and contact area but led to apparent increase in both liner outer maximum contact pressure and contact area. The results of the sliding distance with different initial interferences are shown in Fig. 8.26. It is obvious that the liner rotated with the femoral head at the fixed friction coefficient ratio of 1.48 if the interference was 0. However, even an interference of 25 μm prevented the liner rotating with the head. It means that, when the liner tends to rotate



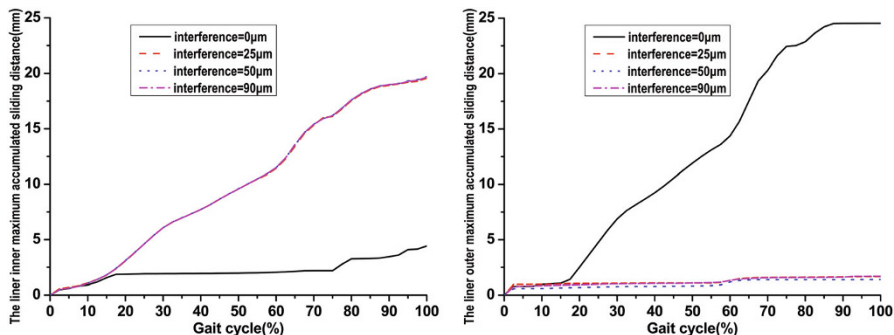


**Fig. 8.26** Maximum accumulated sliding distance of the liner as a function of the gait cycle under different initial interferences of the outer articulation and a fixed friction coefficient ratio of 1.48. (a) Inner maximum accumulated sliding distance. (b) Outer maximum accumulated sliding distance

with the femoral head, it is convenient to prevent its rotation by setting a tiny interference at the outer articulation for dual mobility hip implant.

For dual mobility hip implant, there is another possibility to cause relative sliding of the outer articulation. This may be induced by the contact between stem neck and liner inner rim. Once this happens, the impingement also occurs to UHMWPE liner, and then the liner will rotate with stem until the impingement stops. What's more, the contact between the stem and the UHMWPE liner of the dual mobility hip implant would happen under extreme motions, such as climbing stairs and standing up. Therefore, the dynamic finite element method has been used by Gao et al. to predict the patient movements that led to contact between stem and UHMWPE liner and finally the relative sliding of outer articulation for dual mobility hip implant. The results under chair down/chair up and combining movements are shown in Figs. 8.27, 8.28, 8.29, and 8.30.

It is obvious that contact between the stem neck and the UHMWPE liner inner rim occurred for both cases. The outer accumulating sliding increased with this contact, and the increase of the outer accumulating sliding stopped once the contact ended. Therefore, the dual mobility from different movements of patient after surgery is an unquestionable reason to the dual wear for dual mobility hip implant. However, this contact was rather short during the whole movement, and the outer maximum accumulating sliding distance was much shorter than that of the inner value. This means that the outer wear caused by this case is much lower than that of inner wear. This does not agree with the observations by Geringer et al. [53] and Adam et al. [54] that the outer wear and the inner wear were almost the same. Therefore, more studies are needed to further investigate the true reasons to the wear volume of both articulations for dual mobility hip implant.

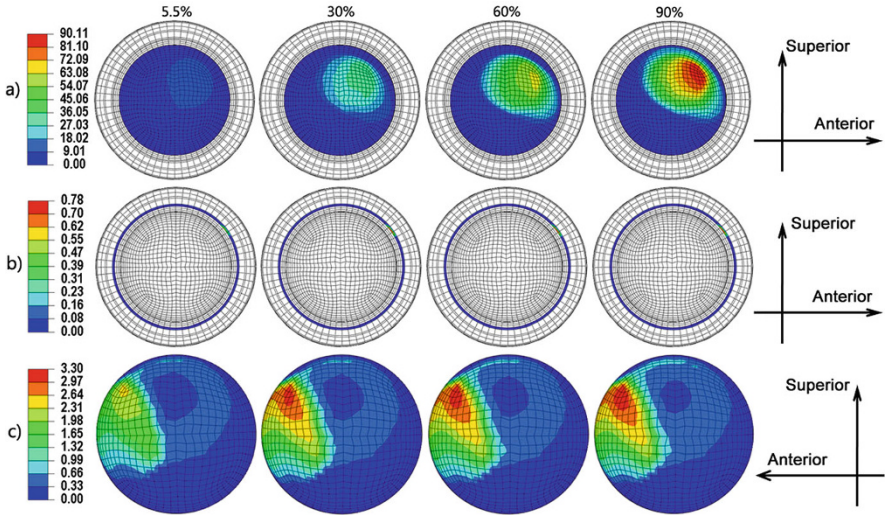


Fig. 8.27 Contours of the liner accumulated sliding distance during different chair down/chair up instants: (a) inner accumulated sliding distance (mm), (b) liner inner rim accumulated sliding distance (mm), and (c) outer accumulated sliding distance (mm)

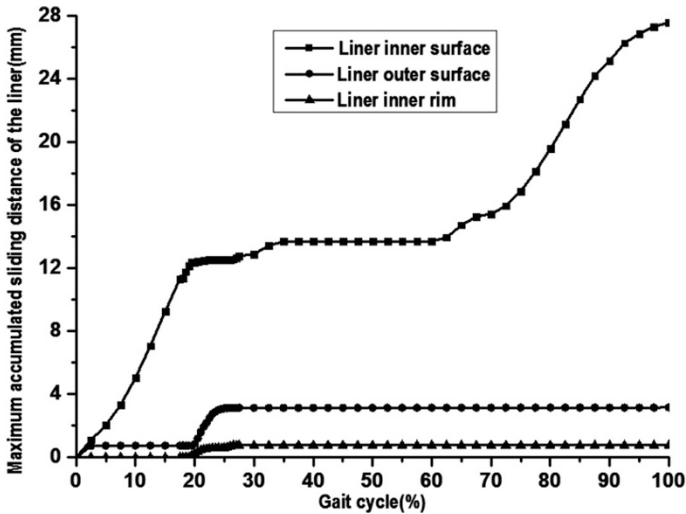
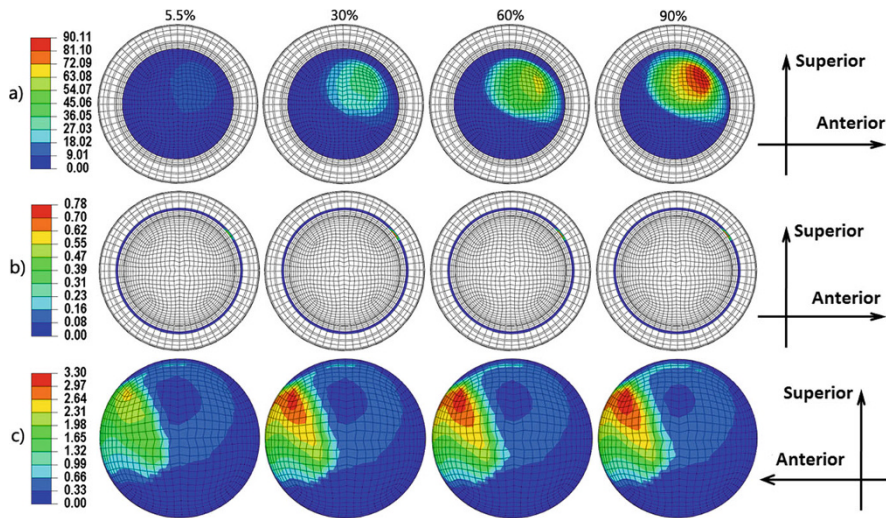
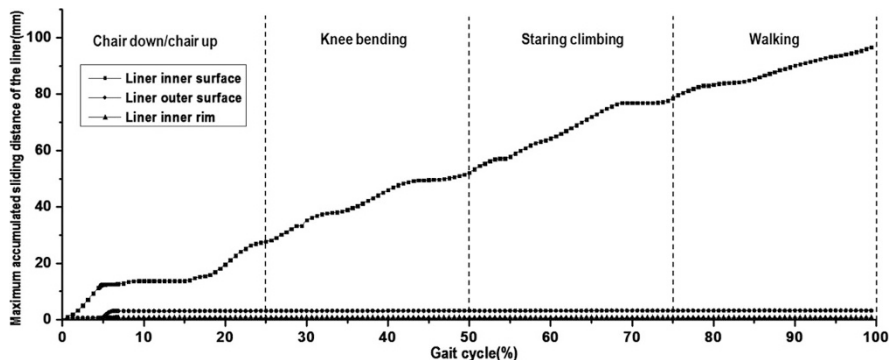


Fig. 8.28 Maximum accumulated sliding distance of the liner as a function of the gait cycle under chair down/chair up movement



**Fig. 8.29** Contours of the liner accumulated sliding distance during combining gait instants: (a) inner accumulated sliding distance (mm), (b) liner inner rim accumulated sliding distance (mm), and (c) outer accumulated sliding distance (mm)



**Fig. 8.30** Maximum accumulated sliding distance of the liner as a function of the gait cycle under combining movements

### 8.3 Biotribology of Artificial Hip Joints

#### 8.3.1 Introduction

Biotribological studies of the bearing surfaces of artificial hip joints include friction, wear, and lubrication, which have been shown to mainly depend on the lubrication regimes involved. There are three lubrication regimes, boundary lubrication, fluid-film lubrication, and mixed lubrication. In the boundary lubrication regime, a significant asperity contact is

experienced, and consequently both friction and wear are high. In the fluid-film lubrication regime where the two bearing surfaces are completely separated by a continuous lubricant, minimal friction and wear are expected. The mixed lubrication regime consists of both fluid-film lubricated and boundary contact regions. Friction and lubrication studies are usually performed to understand the wear mechanism involved in artificial hip joints. However, friction forces may be important in determining the stresses experienced at the interface between the implant and the bone cement [55] as well as temperature rise [56]. The following paragraphs will introduce research on friction, lubrication, and wear of artificial hip joints.

### 8.3.2 Friction

Friction in artificial hip joints is usually measured in a pendulum-like simulator with a dynamic load in the vertical direction and a reciprocating rotation in the horizontal direction. The coefficient of friction is usually expressed as friction factor defined as

$$\mu = \frac{T}{w(d_{\text{head}}/2)} \quad (8.6)$$

where  $T$  is the measured friction torque and  $w$  the load.

The measured coefficient of friction in a particular hip prosthesis itself can generally reveal the nature of the lubrication regime, since each mechanism is associated with broad ranges of the coefficient of friction. The variation in the coefficient of friction against a Sommerfeld number,  $S = (\eta u d_{\text{head}}/w)^{1/2}$ , can further indicate the lubrication regime. If the measured friction factors remain constant, decrease, or increase as the Sommerfeld number increases, the associated modes of lubrication are boundary, mixed, or fluid film, respectively [2].

The experimental studies of metal-on-UHMWPE hip implants by Unsworth et al. [46] clearly indicated boundary or mixed lubrication under steady load, although a suddenly applied load was found to invoke squeeze-film lubrication action. Similar conclusions were drawn by O'Kelly et al. [47] under dynamic loading conditions. In a study by Scholes and Unsworth [57] in 2000, a simple harmonic oscillatory motion and dynamic loading were applied in a hip function simulator. The results indicated that the friction factors were in the range 0.02–0.06 for 28 mm diameter femoral heads and UHMWPE cups, which are representative of mixed lubrication. Then a study by Banchet et al. [58] in 2007 tested the friction coefficients for different materials vs UHMWPE, and the results are shown in Fig. 8.31.

Figure 8.32 shows the friction factor of metal-on-UHMWPE artificial hip joints by different manufacturers by using Leeds ProSim hip simulator. It can be seen that the friction factor fluctuated during the whole walking process in both F/E and A/A orientations.

---

<sup>1</sup>Where  $\eta$  is viscosity and  $u$  velocity

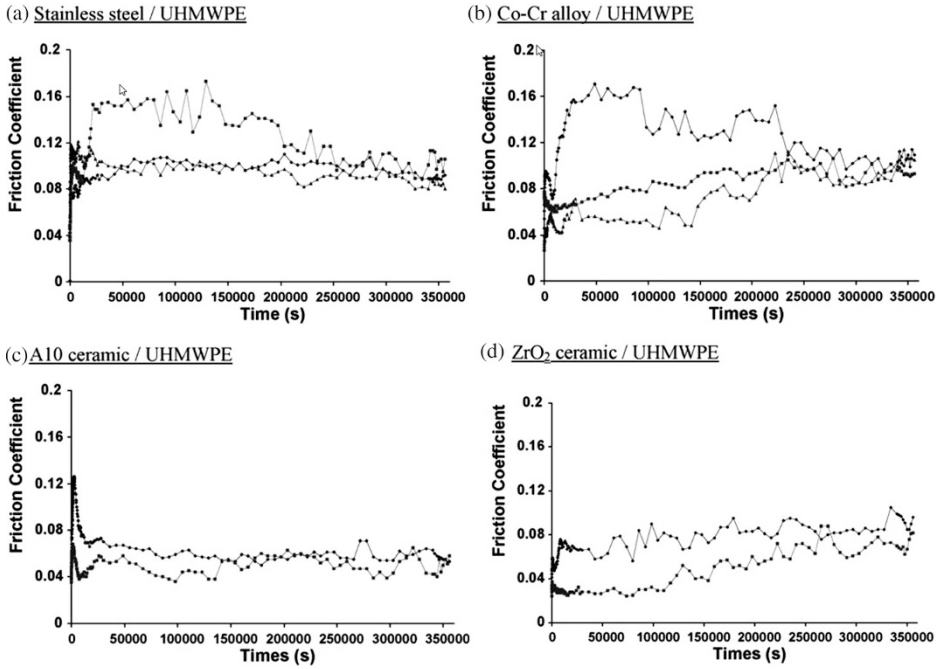


**Fig. 8.31** Friction coefficient evolutions vs time. (Reprinted from Ref. [58], Copyright 2007, with permission from Elsevier)

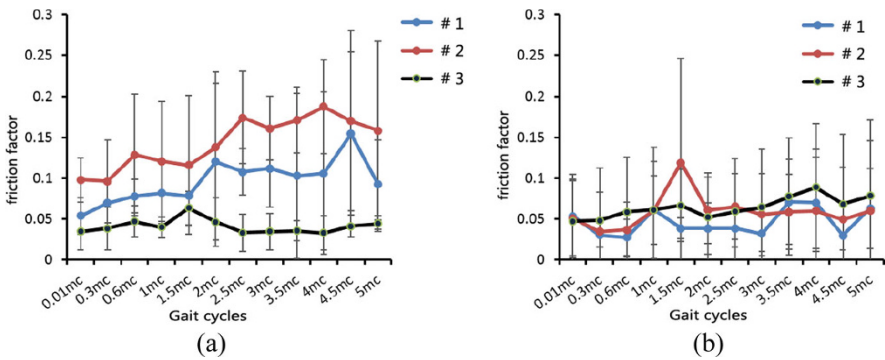


**Fig. 8.32** Friction factor (mean  $\pm$  SD) variation in (a) FE and (b) AA during walking by Leeds ProSim hip simulator

### 8.3.3 Lubrication

Lubrication studies of artificial hip joints are generally carried out using both experimental and theoretical approaches. The experimental measurement usually involves the detection of the separation between the two bearing surfaces using a simple resistivity technique. A large resistance may imply a thick lubricant film, while a small resistance is attributed to the direct surface contact. Such a technique is directly applicable to metal-on-metal bearings as well as metal-on-UHMWPE and ceramic-on-ceramic bearings if appropriate coatings are used [59]. The theoretical analysis generally involves the solution to the Reynolds equation, together with the elasticity equation subjected to the dynamic load and speed experienced during walking. The predicted film thickness ( $h_{\min}$ ) is then compared with the average surface roughness ( $Ra$ ) using the following simple criterion:

$$\lambda = \frac{h_{\min}}{[Ra_{\text{head}}^2 + Ra_{\text{cup}}^2]^{1/2}} \quad (8.7)$$

The lubrication regime is then classified as fluid film, mixed, or boundary if the predicted  $\lambda$  is greater than 3, between 1 and 3, or less than 1, respectively.

Fluid-film lubrication studies in metal-on-UHMWPE hip implants have been largely based on the elastohydrodynamic mechanism associated with the relatively compliant polyethylene material. Initial attempts to predict the lubricating film thickness were made by using an equivalent ball-on-plane configuration with the equivalent radius, a quasi-static condition, and a semi-infinite solid model, and the Hamrock and Dowson [60] film thickness formulae were applied accordingly [59]. The effects of the ball-in-socket configuration and the finite thickness of the acetabular cup were subsequently examined, initially under quasi-static conditions [61] and later extended to transient walking conditions [14]. It was shown that the average of the predicted transient lubricating film thickness over one normal walking cycle was remarkably close to that estimated under the quasi-static condition based on the average load and speed. The predicted average lubricating film thickness was in the range between 0.1 and 0.2  $\mu\text{m}$ . Therefore, a mixed lubrication regime was predicted, since typical average surface roughness between 0.1 and 1  $\mu\text{m}$  has been reported for UHMWPE bearing surfaces [62]. This also demonstrates the importance of the mixed lubrication analysis of metal-on-UHMWPE hip implants.

### 8.3.4 Wear

Our current understanding of the mechanisms of wear particle-induced osteolysis has been developed from over 30 years' experience with metal-on-UHMWPE

implants. The major factors limiting the longevity of initially well-fixed UHMWPE total joint replacements are osteolysis and aseptic loosening [63]. There are evidences from *in vivo* and *in vitro* studies that osteolysis is an UHMWPE particle-related phenomenon.

After total hip arthroplasty, a pseudo-capsule forms around the joint, and this may have a pseudo-synovial lining. A thin fibrous interfacial tissue with few vessels or cells may form at the bone–cement or bone–prosthesis interface [64]. At revision surgery for aseptic loosening, the fibrous membrane is thickened and highly vascularized and contains a heavy infiltrate of UHMWPE-laden macrophages and multinucleated giant cells [65]. There is a correlation between the number of macrophages and the volume of UHMWPE wear debris in the tissues adjacent to areas of aggressive osteolysis [66, 67]. There is a direct relationship between the particle concentration and the duration the implant, and there are billions of particles generated per gram of tissue [68, 69]. Osteolysis likely occurs when the threshold of particles exceeds  $1 \times 10^{10}$  per gram of tissue [67]. Each mg of polyethylene wear has been estimated to generate  $1.3 \times 10^{10}$  particles [68].

The UHMWPE particles isolated from retrieved tissues vary in size and morphology, from large platelet-like particles up to 250  $\mu\text{m}$  in length, fibrils, shreds, and sub-micrometer globule-shaped spheroids 0.1–0.5  $\mu\text{m}$  in diameter [68, 70]. The vast majority of particles are the globular spheroids, and the most frequent distribution is about 0.1–0.5  $\mu\text{m}$ , although the larger particles may account for a high proportion of the total volume of wear debris. Analysis of the mass distribution as a function of size is therefore necessary to discriminate between patient samples [68, 71]. UHMWPE wear particles generated *in vitro* in hip simulators have a larger proportion of the mass of particles in the 0.01–1  $\mu\text{m}$ -sized range than those isolated from periprosthetic tissues [71, 72]. This may indicate that *in vivo*, the smaller particles are disseminated more widely away from the implant site. Recently, improvements to particle imaging techniques have revealed nanometer-sized UHMWPE particles generated in hip simulators. These particles have yet to be identified *in vivo*. These nanometer-size particles account for the greatest number of particles generated but a negligible proportion of the total volume [73].

Studies of the response of macrophages to clinically relevant, endotoxin-free polyethylene particles *in vitro* have clearly demonstrated that particle-stimulated macrophages elaborate a range of potentially osteolytic mediators and bone resorbing activity [74–78]. The activity to induce bone resorption in particle-stimulated macrophage supernatants has been shown dependent on particle size and concentration with particles in the 0.1–1.0  $\mu\text{m}$  size range at a volumetric concentration of 10–100  $\text{m}^3$  per cell, which are the most biologically reactive [74, 76]. This effect of UHMWPE particle size on osteolysis has been demonstrated in animal studies [79]. These findings have enabled preclinical prediction of the functional biological activity of different polyethylenes by analyzing the wear rate and mass distribution of the particles as a function of particle size [72, 80].

### 8.3.4.1 Wear Test

Wear of artificial hip joints has been investigated extensively, due to its direct relevance to biological reactions and clinical problems of osteolysis and loosening. Volumetric wear and wear particles can be measured using the following machines:

- (a) Pin-on-disc machine
- (b) Pin-on-plate machine
- (c) Hip joint simulators

A unidirectional sliding motion is usually used in the pin-on-disc machine, and the reciprocating motion is added to the pin-on-plate machine. Both of these machines are used to screen potential bearing materials under well-controlled and often simplified conditions. Generally, it is necessary to introduce additional motion in order to produce a multidirectional motion. Using this simple device, wear rate could be tested for different material combinations. For metal-on-UHMWPE hip implants, both linear wear rate and volumetric wear rate were tested. The volumetric wear rate of metal-on-UHMWPE was about  $1.066 \times 10^{-6} \text{mm}^3 \text{N}^{-1} \text{m}^{-1}$  by Maxian [81] and Teoh [82].

The next stage of wear testing is usually carried out in hip joint simulators with a varied degree of complexity of the three-dimensional loading and motion patterns experienced by hip joints while immersing the test joints in a lubricant mimicking the synovial fluid. Wear can be evaluated by either dimensional or gravimetric means. Representative commercial hip joint simulators of HUT-4 and Leeds ProSim are shown in Fig. 8.33. These simulators are consisted of at least six stations that operate simultaneously.

Through wear testing, both weight loss and morphology of wear debris could be investigated. When UHMWPE was combined with different materials, the wear rate varied a lot according to Buford et al. [83], as shown in Fig. 8.34. The 316 L steel has the highest wear depth, and the Co–Cr–Mo has the highest wear resistance. Wear volume of conventional and  $\gamma$ -irradiated UHMWPE has been tested [85] (Fig. 8.35). The wear volume of highly cross-linked UHMWPE was much lower than that of conventional UHMWPE. Essner et al. [84] demonstrated that the majority length of wear debris was at the range of 0.1~1  $\mu\text{m}$  (Fig. 8.36).



Fig. 8.33 Hip simulators (a) HUT-4 and (b) Leeds ProSim



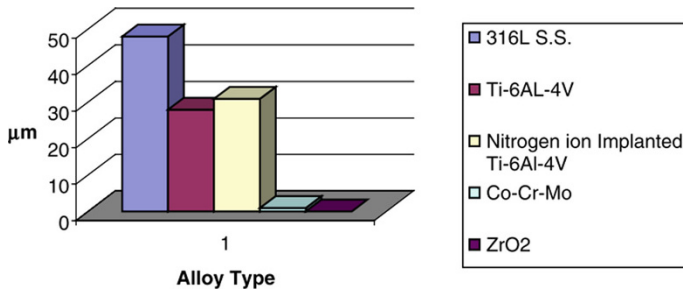


**Fig. 8.34** Wear depth in various biomaterials. (Reprinted from Ref. [83], Copyright 2004, with permission from Elsevier)

**Fig. 8.35** Hip simulator wear comparison of non-radiated and  $\gamma$ -irradiation in air UHMWPE cups. (Reprint for Ref. [85], Copyright 2005, with permission from Elsevier)

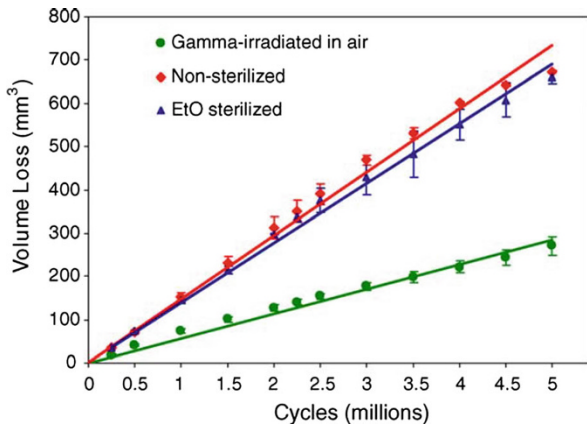


**Fig. 8.36** Hip simulator Duration<sup>®</sup> UHMWPE acetabular liner wear debris. (Reprinted from Ref. [84], Copyright 2005, with permission from Elsevier)



Oral et al. [86] tested wear loss and measured wear trace of artificial hip joints of different UHMWPE materials. The result of wear loss for different UHMWPE materials is shown in Fig. 8.37. The wear loss of UHMWPE sharply decreased if

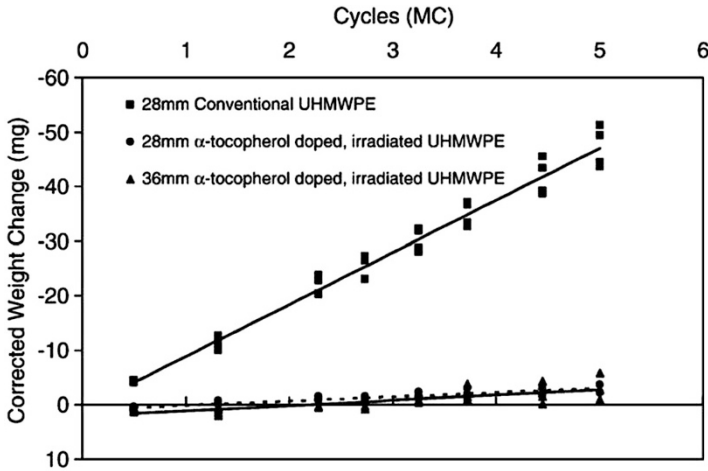


**Fig. 8.37** Average total weight change of tested liners ( $n = 4$ ) corrected for fluid absorption shown with corresponding linear regression lines. (Reprinted from Ref. [85], Copyright 2006, with permission from Elsevier)

it was irradiated. Besides, there were still machining marks on irradiated UHMWPE surface, while this was polished for conventional UHMWPE cup surface, as shown in Fig. 8.38.

Hip simulator indeed could test both wear volume and morphology of artificial hip joints, and experimental data are consistent with clinic outcomes. However, wear test is rather time-consuming; a short-term test of 5 million walking gait cycle will last at least 3 months. Besides, it is also somewhat expensive. Furthermore, it is hard to use this method to do parametric studies. Thus, wear numerical computation has been introduced and widely used to predict wear of artificial hip joints.

#### 8.3.4.2 Wear Numerical Computation

The numerical method of wear prediction for artificial hip joints was firstly introduced by Maxian et al. [81] in 1996. In that study, the Archard's wear law was used to calculate wear depth and volume of UHMWPE cup, and corresponding data were about 0.1 mm/year and 15 mm<sup>3</sup>/year, respectively. In the first wear model, because wear rate UHMWPE was assumed constant, it could only be used to predict wear of the artificial hip used by Maxian et al. [81]. However, since this numerical method was introduced, parametric analysis of wear for artificial hip joints has become available. Then, the elastic-plastic property of UHMWPE is considered for the wear numerical computation for metal-on-UHMWPE artificial hip joints. Besides, parameters that could affect wear rate of UHMWPE material are taken into account in the wear rate derived, such as contact pressure, surface roughness, and sliding velocity. The procedure of that numerical method could be illustrated by using the following flowchart in Fig. 8.39.

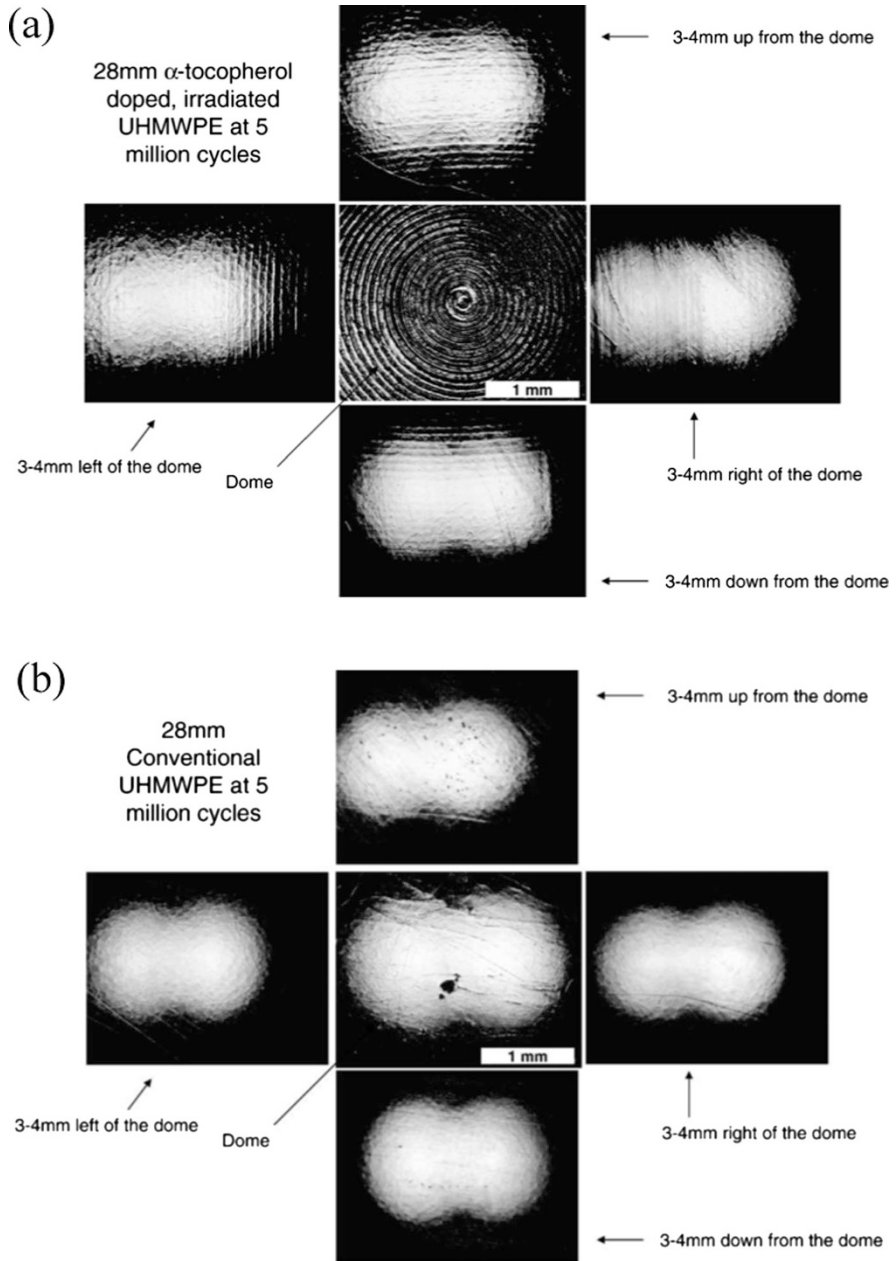


**Fig. 8.38** Compilation of photos showing a 28-mm vitamin E doped, (a) irradiated, and (b) conventional UHMWPE liner after 5Mc of testing on the hip simulator. Machining marks are present in all four quadrants and also at the dome. (Reprinted from Ref. [85], Copyright 2006, with permission from Elsevier)

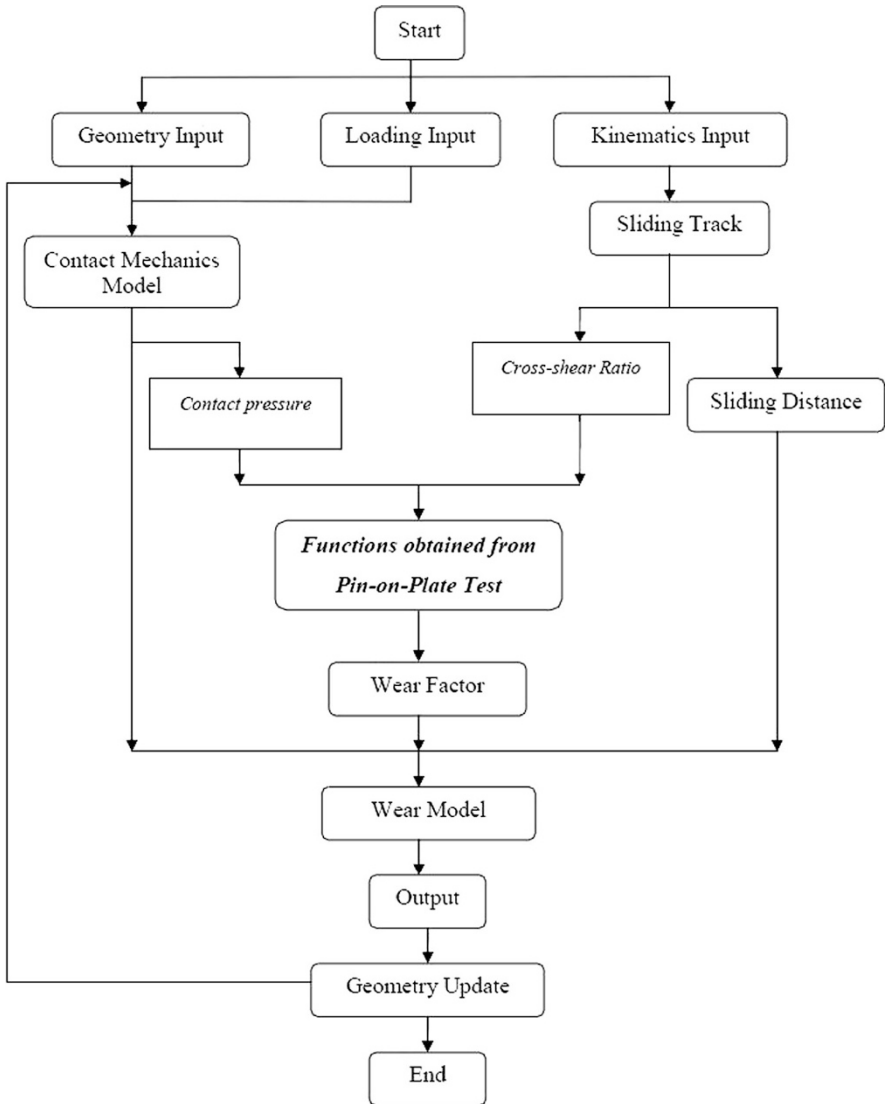
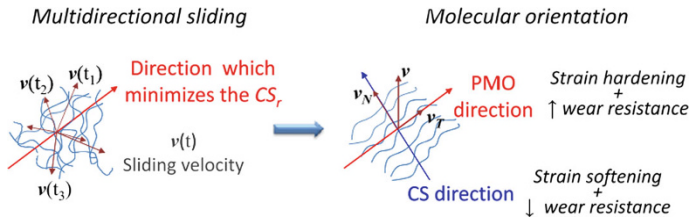


Fig. 8.39 Computational and experimental elements in wear simulation

The effect of multidirectional sliding of artificial hip joints on the wear of UHMWPE cups has been considered. According to experimental observations, the polymeric chains of UHMWPE acquire a principal molecular orientation (PMO) and are thus hardened along this direction, which makes the polymers harder to fail and wear. In contrast, in the direction perpendicular to the PMO, there is a strain softening phenomenon which is predominantly responsible for the detachment of fibrous wear debris from the worn surfaces (Fig. 8.40). Thus, the so-called cross-



**Fig. 8.40** Schematic representation of the cross-shear effect. UHMWPE polymeric chain, initially randomly oriented (a) and reoriented in the PMO direction because of multidirectional sliding on a harder counterface (b). (Reprinted from ref. [86], Copyright 2008, with permission from Elsevier)

shear ratio,  $CS$ , is defined to represent the effect of this multi-direction motion on wear rate of UHMWPE. The cross-shear ratio,  $CS$ , could be determined by frictional work released perpendicular to the PMO dividing the total frictional work.

The latest studies by Kang et al. [86, 87] and Liu et al. [44] have further developed the method to calculate cross-shear ratio,  $CS$ , and the wear coefficient  $k_c$  (or wear factor  $k_f$ ) that is related to  $CS$ . When different forces and rotation motions are used, the  $CS$  distributions could be predicted for UHMWPE cup, as described by Mattei et al. (Fig. 8.41). It can be seen that wear coefficient (or wear factor) would increase with increasing  $CS$ .

Kang et al. also compared both  $CS$  and wear volume of conventional and highly cross-linked UHMWPE artificial hip joints [88]. The relationship between wear factor and  $CS$  for different UHMWPE materials is shown in Fig. 8.42. The wear factor under same  $CS$  of conventional UHMWPE was much higher than that of highly cross-linked UHMWPE. The wear volume results by Kang for both UHMWPE materials are shown in Fig. 8.43. It is obvious that the wear volume of conventional UHMWPE under same conditions was much higher than that of highly cross-linked UHMWPE.

By using different wear laws, both wear depth and volume could be calculated, and the corresponding data by Mattei et al. [89] are shown in Fig. 8.44. It can be seen both wear depth and wear volume are different by using different wear coefficients (or wear factors) in spite of the nearly same wear zones.

Liu et al. [90] also used a new wear law introduced by themselves to predict wear volume of UHMWPE with creep considered, only to find that the total wear volume of UHMWPE cup sharply increased.

## 8.4 Conclusions and Future Trends

### 8.4.1 Conclusions

The UHMWPE artificial hip joint is widely used in clinic, but wear performance limits its long-term usage. This chapter has introduced attempts to enhance the

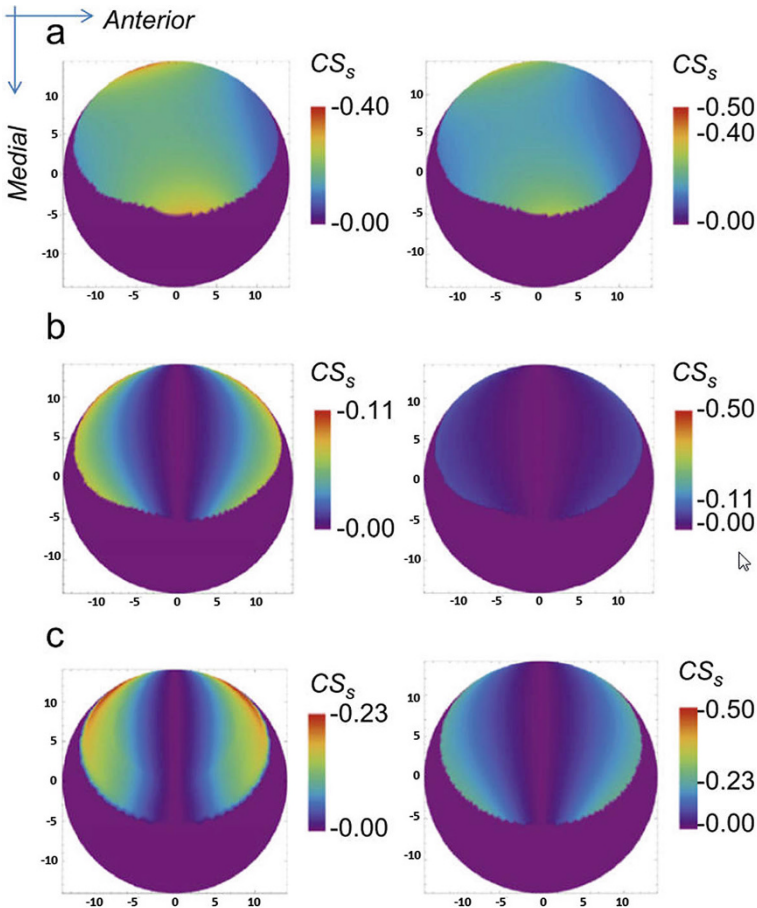


**Fig. 8.41**  $CS_s$  maps for three different kinematics conditions: complete in vivo gait velocity (a), simplified case with  $\omega_y - \omega_y$  (b), and Leeds ProSim simulator (c). In the left column, each plot is represented within its own minimum and maximum values, while in the right column all the  $CS_s$  plots are depicted in the same range (0–0.5). (Reprinted from Ref. [86], Copyright 2013, with permission from Elsevier)

UHMWPE cup wear resistance ability and research on wear mechanism and performance from both biomechanics and biotribology. The main conclusions obtained from these studies can be mainly summarized as:

- (a) The musculoskeletal multibody dynamics of the UHMWPE hip implant is necessary, and both hip joint center and surgical approach would influence hip contact force; thus the hip implant position and surgical approach should be considered according to patient during surgery.
- (b) The finite element method has been widely used to investigate both contact mechanics and kinematics. The contact pressure and contact area are related to

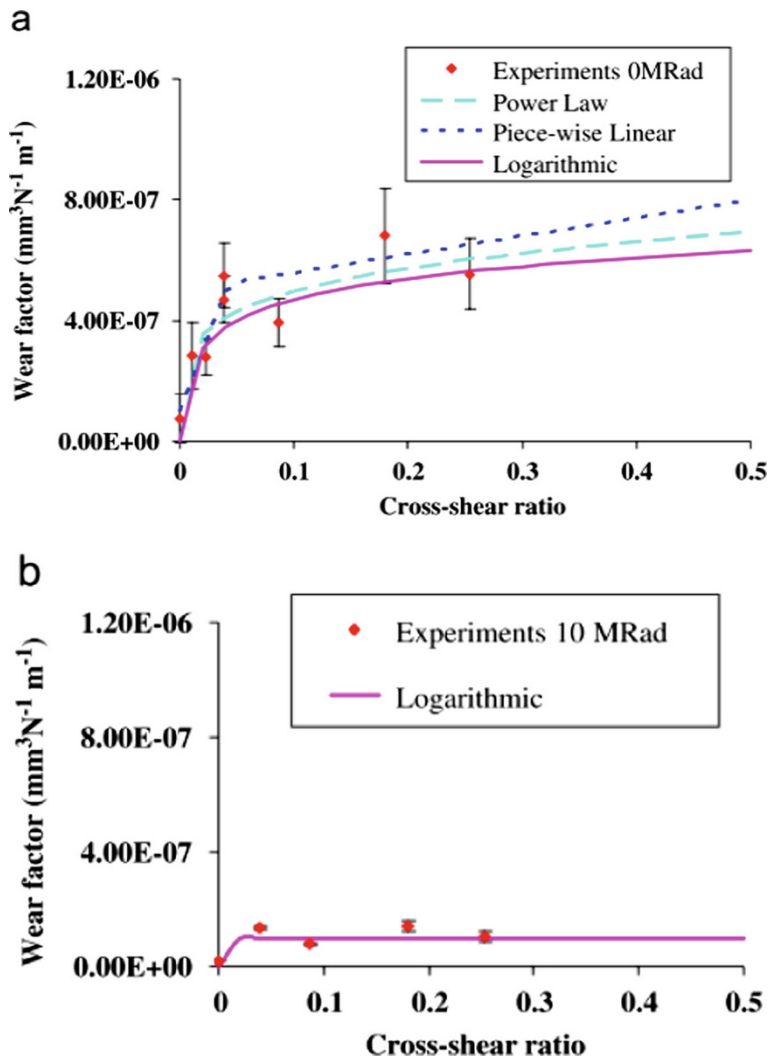
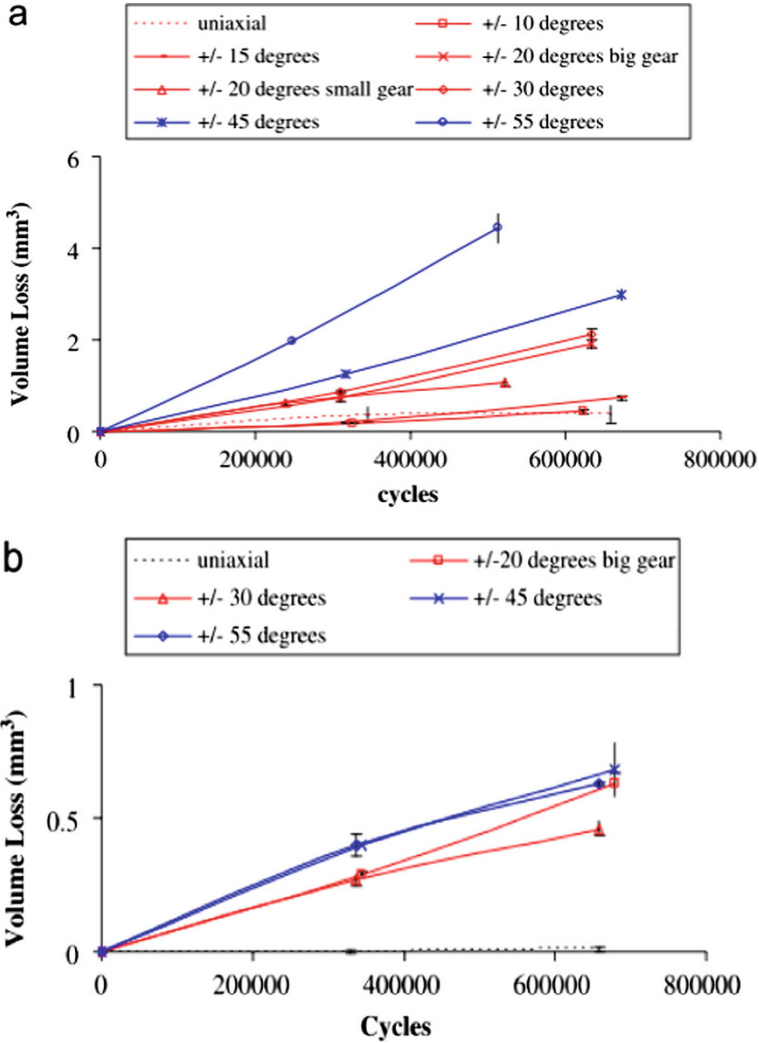


Fig. 8.42 Wear factor versus average cross-shear ratio for (a) 0 MRad conventional UHMWPE and (b) 10 MRad highly cross-linked UHMWPE (dispersion bar: mean ( $n \geq 3$ )  $\pm$  95% CI) [88]

hip contact force, clearance/interference, friction coefficient, and so on, while the sliding distance would be mainly affected by patient movements.

- (c) Biotribology performances including friction, lubrication, and wear of the UHMWPE hip implant have been widely investigated; the UHMWPE hip implant experiences boundary lubrication, and its wear volume is different for the conventional UHMWPE and the high cross-linked UHMWPE material.



**Fig. 8.43** Volume loss at various stages of cycles for (a) 0 MRad conventional UHMWPE and (b) 10 MRad highly cross-linked UHMWPE (dispersion bar: mean ( $n \geq 3$ )  $\pm$  95% CI) [88]

### 8.4.2 Future Trends

Currently, much research has been done to understand wear mechanisms and improve its resistant performance as represented in this chapter. However, longer lifetime is expected in the future for the UHMWPE hip implant because of diverse demands from young and active patients. This may be achieved by the following attempts:



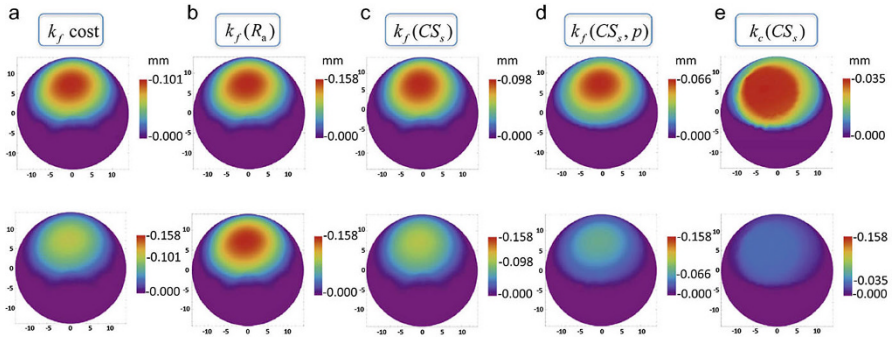


**Fig. 8.44** Acetabular cup linear wear maps (in the  $x_c$ - $y_c$  plane) and volumetric wear after 1Mc are predicted using different wear laws, under in vivo gait conditions. (Reprinted from Ref. [89], Copyright 2013, with permission from Elsevier)

#### (a) Improvement of Wear Performance of the UHMWPE Material

As done in the past decades, both wear depth and wear volume of the UHMWPE hip implant have been dramatically decreased by replacing conventional UHMWPE material with highly cross-linked UHMWPE material. In the future, the UHMWPE with even lower wear could be expected.

#### (b) Individual Preoperative Surgical Planning

The wear performance of an UHMWPE hip implant is related to the prosthesis design, surgical accuracy, and patient characteristics. Therefore, it is better to simulate wear performance of the hip implant before surgery using the current computational methods to predict the optimal parameters to guide the surgery.

## References

1. Gluscevic BM, Kraljevic BD, Jovanovic VA, Stosic PB, Milosavljevic DM, Radivojevic RM (2006) Primary total hip arthroplasty in patients with rheumatoid arthritis. *Acta Chir Lugosl* 53 (4):4
2. Dowson D (2001) New joints for the millennium: wear control in total replacement hip joints. *Proc Inst Mech Eng H J Eng Med* 215(4):335–358
3. De Martino I, Triantafyllopoulos GK, Sculco PK, Sculco TP (2014) Dual mobility cups in total hip arthroplasty. *World J Orthop* 5(3):180–187. <https://doi.org/10.5312/wjo.v5.i3.180>
4. Tarabolsi M, Klassen T, Mantwill F, Gartner F, Siegel F, Schulz AP (2013) Patterned CoCrMo and Al O surfaces for reduced free wear debris in artificial joint arthroplasty. *J Biomed Mater Res A* 101(12):3447–3456. <https://doi.org/10.1002/jbm.a.34644>
5. Ge S, Wang S, Huang X (2009) Increasing the wear resistance of UHMWPE acetabular cups by adding natural biocompatible particles. *Wear* 267(5–8):770–776. <https://doi.org/10.1016/j.wear.2009.01.057>
6. Dumbleton JH, Manley MT (2005) Metal-on-metal total hip replacement: what does the literature say? *J Arthroplast* 20(2):174–188

7. Greene JW, Malkani AL, Kolisek FR, Jessup NM, Baker DL (2009) Ceramic-on-ceramic total hip arthroplasty. *J Arthroplast* 24(6 Suppl):15–18. <https://doi.org/10.1016/j.arth.2009.04.029>
8. Lindeque B, Hartman Z, Noshchenko A, Cruse M (2014) Infection after primary total hip arthroplasty. *Orthopedics* 37(4):257–265. <https://doi.org/10.3928/01477447-20140401-08>
9. Berry DJ, von Knoch M, Schleck CD, Harmsen WS (2004) The cumulative long-term risk of dislocation after primary Charnley total hip arthroplasty. *J Bone Joint Surg Am* 86-A(1):9–14
10. Kosashvili Y, Drexler M, Backstein D, Safir O, Lakstein D, Safir A, Chakraverty R, Dwyer T, Gross A (2014) Dislocation after the first and multiple revision total hip arthroplasty: comparison between acetabulum-only, femur-only and both component revision hip arthroplasty. *Can J Surg/Journal canadien de chirurgie* 57(2):E15–E18
11. Carriero A, Zavatsky A, Stebbins J, Theologis T, Lenaerts G, Jonkers I, Shefelbine SJ (2014) Influence of altered gait patterns on the hip joint contact forces. *Comput Methods Biomech Biomed Engin* 17(4):352–359. <https://doi.org/10.1080/10255842.2012.683575>
12. Schwachmeyer V, Damm P, Bender A, Dymke J, Graichen F, Bergmann G (2013) In vivo hip joint loading during post-operative physiotherapeutic exercises. *PLoS One* 8(10):e77807. <https://doi.org/10.1371/journal.pone.0077807>
13. Seedhom BB, Wallbridge NC (1985) Walking activities and wear of prostheses. *Ann Rheum Dis* 44(12):838–843
14. Jagatia M, Jalali-Vahid D, Jin ZM (2001) Elastohydrodynamic lubrication analysis of ultra-high molecular weight polyethylene hip joint replacements under squeeze-film motion. *Proc Inst Mech Eng H J Eng Med* 215(2):141–152. <https://doi.org/10.1243/0954411011533706>
15. Williams PA, Clarke IC (2009) Understanding polyethylene wear mechanisms by modeling of debris size distributions. *Wear* 267(1–4):646–652. <https://doi.org/10.1016/j.wear.2008.12.069>
16. Ingham E, Fisher J (2005) The role of macrophages in osteolysis of total joint replacement. *Biomaterials* 26(11):1271–1286. <https://doi.org/10.1016/j.biomaterials.2004.04.035>
17. Austin MS, Higuera CA, Rothman RH (2012) Total hip arthroplasty at the rothman institute. *HSS J musculoskelet J Hosp for Spec Surg* 8(2):146–150. <https://doi.org/10.1007/s11420-012-9268-x>
18. Wang L, Liu X, Li D, Liu F, Jin Z (2014) Contact mechanics studies of an ellipsoidal contact bearing surface of metal-on-metal hip prostheses under micro-lateralization. *Med Eng Phys* 36(4):419–424. <https://doi.org/10.1016/j.medengphy.2013.12.017>
19. Saikko V, Calonius O, Keranen J (2004) Effect of slide track shape on the wear of ultra-high molecular weight polyethylene in a pin-on-disk wear simulation of total hip prosthesis. *J Biomed Mater Res B Appl Biomater* 69(2):141–148. <https://doi.org/10.1002/jbm.b.20043>
20. Ong KL, Manley MT, Nevelos J, Greene K (2012) Review: biomechanical issues in total hip replacement. *Surg Technol Int* 22:222–228
21. Heiberg KE, Ekeland A, Bruun-Olsen V, Mengshoel AM (2013) Recovery and prediction of physical functioning outcomes during the first year after total hip arthroplasty. *Arch Phys Med Rehabil* 94(7):1352–1359. <https://doi.org/10.1016/j.apmr.2013.01.017>
22. Alberta Hip Improvement P, MacKenzie JR, O'Connor GJ, Marshall DA, Faris PD, Dort LC, Khong H, Parker RD, Werle JR, Beaupre LA, Frank CB (2012) Functional outcomes for 2 years comparing hip resurfacing and total hip arthroplasty. *J Arthroplast* 27(5):750–757. e752. <https://doi.org/10.1016/j.arth.2011.10.004>
23. Ewen AM, Stewart S, St Clair Gibson A, Kashyap SN, Caplan N (2012) Post-operative gait analysis in total hip replacement patients—a review of current literature and meta-analysis. *Gait Posture* 36(1):1–6. <https://doi.org/10.1016/j.gaitpost.2011.12.024>
24. Jensen C, Aagaard P, Overgaard S (2011) Recovery in mechanical muscle strength following resurfacing vs standard total hip arthroplasty – a randomised clinical trial. *Osteoarthritis Cartil* 19(9):1108–1116. <https://doi.org/10.1016/j.joca.2011.06.011>
25. Damsgaard M, Rasmussen J, Christensen ST, Surma E, de Zee M (2006) Analysis of musculoskeletal systems in the anybody modeling system. *Simul Model Pract Theory* 14(8):1100–1111. <https://doi.org/10.1016/j.simpat.2006.09.001>
26. Ren L, Qian Z, Ren L (2014) Biomechanics of musculoskeletal system and its biomimetic implications: a review. *J Bionic Eng* 11(2):159–175. [https://doi.org/10.1016/S1672-6529\(14\)60033-0](https://doi.org/10.1016/S1672-6529(14)60033-0)

27. Hallaceli H, Uruc V, Uysal HH, Ozden R, Hallaceli C, Soyuer F, Ince Parpucu T, Yengil E, Cavlak U (2014) Normal hip, knee and ankle range of motion in the Turkish population. *Acta Orthop Traumatol Turc* 48(1):37–42. <https://doi.org/10.3944/aott.2014.3113>
28. Delp SL, Anderson FC, Arnold AS, Loan P, Habib A, John CT, Guendelman E, Thelen DG (2007) OpenSim: open-source software to create and analyze dynamic simulations of movement. *IEEE Trans Biomed Eng* 54(11):1940–1950. <https://doi.org/10.1109/tbme.2007.901024>
29. Manders C, New A, Rasmussen J (2008) Validation of musculoskeletal gait simulation for use in investigation of total hip replacement. *J Biomech* 41:S488. [https://doi.org/10.1016/S0021-9290\(08\)70487-1](https://doi.org/10.1016/S0021-9290(08)70487-1)
30. Sherman MA, Seth A, Delp SL (2011) Simbody: multibody dynamics for biomedical research. *Procedia IUTAM* 2:241–261
31. Rydell NW (1966) Forces acting on the femoral head-prosthesis. A study on strain gauge supplied prostheses in living persons. *Acta Orthop Scand* 37(88):1–132
32. Zhang X, Chen Z, Wang L, Yang W, Li D, Jin Z (2015) Prediction of hip joint load and translation using musculoskeletal modelling with force-dependent kinematics and experimental validation. *Proc Inst Mech Eng H J Eng Med* 229(7):477–490. <https://doi.org/10.1177/0954411915589115>
33. Besong AA, Lee R, Farrar R, Jin ZM (2001) Contact mechanics of a novel metal-on-metal total hip replacement. *Proc Inst Mech Eng H J Eng Med* 215(6):543–548. <https://doi.org/10.1243/0954411011536145>
34. Wilson DR, Apreleva MV, Eichler MJ, Harrold FR (2003) Accuracy and repeatability of a pressure measurement system in the patellofemoral joint. *J Biomech* 36(12):1909–1915
35. Muller O, Parak WJ, Wiedemann MG, Martini F (2004) Three-dimensional measurements of the pressure distribution in artificial joints with a capacitive sensor array. *J Biomech* 37(10):1623–1625. <https://doi.org/10.1016/j.jbiomech.2004.01.024>
36. Hua X, Li J, Wang L, Jin Z, Wilcox R, Fisher J (2014) Contact mechanics of modular metal-on-polyethylene total hip replacement under adverse edge loading conditions. *J Biomech* 47(13):3303–3309. <https://doi.org/10.1016/j.jbiomech.2014.08.015>
37. Wang L, Williams S, Udofia I, Isaac G, Fisher J, Jin Z (2012) The effect of cup orientation and coverage on contact mechanics and range of motion of metal-on-metal hip resurfacing arthroplasty. *Proc Inst Mech Eng H J Eng Med* 226(11):877–886. <https://doi.org/10.1177/0954411912456926>
38. Hua X, Wroblewski BM, Jin Z, Wang L (2012) The effect of cup inclination and wear on the contact mechanics and cement fixation for ultra high molecular weight polyethylene total hip replacements. *Med Eng Phys* 34(3):318–325. <https://doi.org/10.1016/j.medengphy.2011.07.026>
39. Liu F (2005) Contact mechanics and elastohydrodynamic lubrication analysis of metal-on-metal hip implant with a sandwich acetabular cup under transient walking condition. University of Bradford
40. Beaulé PE, Amstutz HC (2005) Orientation of the femoral component in surface arthroplasty of the hip. *J Bone Joint Surg Am* 87(5):1162
41. Brodner W, Grubl A, Jankovsky R, Meisinger V, Lehr S, Gottsauner-Wolf F (2004) Cup inclination and serum concentration of cobalt and chromium after metal-on-metal total hip arthroplasty. *J Arthroplast* 19(8 Suppl 3):5
42. Isaac GH, Siebel T, Oakeshott RD, McLennan-Smith R, Cobb AG, Schmalzried TP, Vail TP (2009) Changes in whole blood metal ion levels following resurfacing: serial measurements in a multi-centre study. *Hip Int J Clin Exp Res Hip Pathol Ther* 19(4):330–337
43. Kang L, Galvin AL, Jin ZM, Fisher J (2006) A simple fully integrated contact-coupled wear prediction for ultra-high molecular weight polyethylene hip implants. *Proc Inst Mech Eng H J Eng Med* 220(1):33–46
44. Liu F, Leslie I, Williams S, Fisher J, Jin Z (2008) Development of computational wear simulation of metal-on-metal hip resurfacing replacements. *J Biomech* 41(3):686–694. <https://doi.org/10.1016/j.jbiomech.2007.09.020>

45. Wang L, Yang W, Peng X, Li D, Dong S, Zhang S, Zhu J, Jin Z (2015) Effect of progressive wear on the contact mechanics of hip replacements – does the realistic surface profile matter? *J Biomech* 48(6):1112–1118. <https://doi.org/10.1016/j.jbiomech.2015.01.020>
46. Saikko V, Calonius O (2002) Slide track analysis of the relative motion between femoral head and acetabular cup in walking and in hip simulators. *J Biomech* 35:10
47. Gao Y, Jin Z, Wang L, Wang M (2015) Finite element analysis of sliding distance and contact mechanics of hip implant under dynamic walking conditions. *Proc Inst Mech Eng H J Eng Med* 229(6):469–474. <https://doi.org/10.1177/09544119155585380>
48. Craig JJ (1989) *Introduction to robotics: mechanics and control*. Addison-Wesley, Reading
49. Guyen O, Pibarot V, Vaz G, Chevillotte C, Bejui-Hugues J (2009) Use of a dual mobility socket to manage total hip arthroplasty instability. *Clin Orthop Relat Res* 467(2):465–472. <https://doi.org/10.1007/s11999-008-0476-0>
50. Philippot R, Adam P, Farizon F, Fessy MH, Bousquet G (2006) Survival of cementless dual mobility sockets: ten-year follow-up. *Revue de chirurgie orthopedique et reparatrice de l'appareil moteur* 92(4):326–331
51. Philippot R, Camilleri JP, Boyer B, Adam P, Farizon F (2009) The use of a dual-articulation acetabular cup system to prevent dislocation after primary total hip arthroplasty: analysis of 384 cases at a mean follow-up of 15 years. *Int Orthop* 33(4):927–932. <https://doi.org/10.1007/s00264-008-0589-9>
52. Gao Y, Chai W, Wang L, Wang M, Jin Z (2016) Effect of friction and clearance on kinematics and contact mechanics of dual mobility hip implant. *Proc Inst Mech Eng H J Eng Med* 230(1):39–49. <https://doi.org/10.1177/0954411915617198>
53. Geringer J, Boyer B, Farizon F (2011) Understanding the dual mobility concept for total hip arthroplasty. Investigations on a multiscale analysis-highlighting the role of arthrofibrosis. *Wear* 271(9–10):2379–2385. <https://doi.org/10.1016/j.wear.2011.02.027>
54. Adam P, Farizon F, Fessy MH (2005) Dual articulation retentive acetabular liners and wear: surface analysis of 40 retrieved polyethylene implants. *Revue de chirurgie orthopedique et reparatrice de l'appareil moteur* 91(7):10
55. Nassutt R, Wimmer MA, Schneider E, Morlock MM (2003) The influence of resting periods on friction in the artificial hip. *Clin Orthop Relat Res* 407:127–138
56. Bergmann G, Graichen F, Rohlmann A, Verdonschot N, van Lenthe GH (2001) Frictional heating of total hip implants. Part 2: finite element study. *J Biomech* 34(4):429–435
57. Scholes SC, Unsworth A (2000) Comparison of friction and lubrication of different hip prostheses. *Proc Inst Mech Eng H J Eng Med* 214(1):49–57. <https://doi.org/10.1243/0954411001535237>
58. Banchet V, Fridrici V, Abry JC, Kapsa P (2007) Wear and friction characterization of materials for hip prosthesis. *Wear* 263(7–12):1066–1071. <https://doi.org/10.1016/j.wear.2007.01.085>
59. Jin ZM, Dowson D, Fisher J (1997) Analysis of fluid film lubrication in artificial hip joint replacements with surfaces of high elastic modulus. *Proc Inst Mech Eng H J Eng Med* 211(3):247–256. <https://doi.org/10.1243/0954411971534359>
60. Hamrock BJ, Dowson D (1978) Elastohydrodynamic lubrication of elliptical contacts for materials of low elastic modulus. I: fully flooded conjunction. *Trans ASME J Lubric Technol* 100(2):236–245
61. Jalali-Vahid D, Jagatia M, Jin ZM, Dowson D (2001) Prediction of lubricating film thickness in UHMWPE hip joint replacements. *J Biomech* 34(2):261–266
62. Elfick AP (1998) Surface topography of retrieved PCA acetabular liners: proposal for a novel wear mechanism. *J Mater Sci Lett* 17(13):1085–1088
63. Engh CA Jr, Hopper RH Jr, Huynh C, Ho H, Sritulanondha S, Engh CA Sr (2012) A prospective, randomized study of cross-linked and non-cross-linked polyethylene for total hip arthroplasty at 10-year follow-up. *J Arthroplast* 27(8 Suppl):2–7. e1. <https://doi.org/10.1016/j.arth.2012.03.048>
64. Goldring SR, Schiller AL, Roelke M, Rourke CM, O'Neil DA, Harris WH (1983) The synovial-like membrane at the bone-cement interface in loose total hip replacements and its proposed role in bone lysis. *J Bone Joint Surg Am* 65(5):575–584

65. Mirra JM, Marder RA, Amstutz HC (1982) The pathology of failed total joint arthroplasty. *Clin Orthop Relat Res* 170:175–183
66. Schmalzried TP, Jasty M, Harris WH (1992) Periprosthetic bone loss in total hip arthroplasty. Polyethylene wear debris and the concept of the effective joint space. *J Bone Joint Surg Am* 74 (6):849–863
67. Revell PA, al-Saffar N, Kobayashi A (1997) Biological reaction to debris in relation to joint prostheses. *Proc Inst Mech Eng H J Eng Med* 211(2):187–197. <https://doi.org/10.1243/0954411971534304>
68. Tipper JL, Ingham E, Hailey JL, Besong AA, Fisher J, Wroblewski BM, Stone MH (2000) Quantitative analysis of polyethylene wear debris, wear rate and head damage in retrieved Charnley hip prostheses. *J Mater Sci Mater Med* 11(2):117–124
69. Hirakawa K, Bauer TW, Stulberg BN, Wilde AH (1996) Comparison and quantitation of wear debris of failed total hip and total knee arthroplasty. *J Biomed Mater Res* 31(2):257–263. [https://doi.org/10.1002/\(SICI\)1097-4636\(199606\)31:2<257::AID-JBM13>3.0.CO;2-I](https://doi.org/10.1002/(SICI)1097-4636(199606)31:2<257::AID-JBM13>3.0.CO;2-I)
70. Maloney WJ, Smith RL, Schmalzried TP, Chiba J, Huene D, Rubash H (1995) Isolation and characterization of wear particles generated in patients who have had failure of a hip arthroplasty without cement. *J Bone Joint Surg Am* 77(9):1301–1310
71. Howling GI, Barnett PI, Tipper JL, Stone MH, Fisher J, Ingham E (2001) Quantitative characterization of polyethylene debris isolated from periprosthetic tissue in early failure knee implants and early and late failure Charnley hip implants. *J Biomed Mater Res* 58(4):415–420
72. Endo M, Tipper JL, Barton DC, Stone MH, Ingham E, Fisher J (2002) Comparison of wear, wear debris and functional biological activity of moderately crosslinked and non-crosslinked polyethylenes in hip prostheses. *Proc Inst Mech Eng H J Eng Med* 216(2):111–122. <https://doi.org/10.1243/0954411021536333>
73. Ingram JH, Stone M, Fisher J, Ingham E (2004) The influence of molecular weight, crosslinking and counterface roughness on TNF-alpha production by macrophages in response to ultra high molecular weight polyethylene particles. *Biomaterials* 25(17):3511–3522. <https://doi.org/10.1016/j.biomaterials.2003.10.054>
74. Green TR, Fisher J, Matthews JB, Stone MH, Ingham E (2000) Effect of size and dose on bone resorption activity of macrophages by in vitro clinically relevant ultra high molecular weight polyethylene particles. *J Biomed Mater Res* 53(5):490–497
75. Matthews JB, Green TR, Stone MH, Wroblewski BM, Fisher J, Ingham E (2000) Comparison of the response of primary human peripheral blood mononuclear phagocytes from different donors to challenge with model polyethylene particles of known size and dose. *Biomaterials* 21 (20):2033–2044
76. Green TR, Fisher J, Stone M, Wroblewski BM, Ingham E (1998) Polyethylene particles of a ‘critical size’ are necessary for the induction of cytokines by macrophages in vitro. *Biomaterials* 19(24):2297–2302
77. Matthews JB, Green TR, Stone MH, Wroblewski BM, Fisher J, Ingham E (2000) Comparison of the response of primary murine peritoneal macrophages and the U937 human histiocytic cell line to challenge with in vitro generated clinically relevant UHMWPE particles. *Biomed Mater Eng* 10(3–4):229–240
78. Matthews JB, Green TR, Stone MH, Wroblewski BM, Fisher J, Ingham E (2001) Comparison of the response of three human monocytic cell lines to challenge with polyethylene particles of known size and dose. *J Mater Sci Mater Med* 12(3):249–258
79. Goodman SB, Fornasier VL, Lee J, Kei J (1990) The histological effects of the implantation of different sizes of polyethylene particles in the rabbit tibia. *J Biomed Mater Res* 24(4):517–524. <https://doi.org/10.1002/jbm.820240408>
80. Fisher J, Bell J, Barbour PS, Tipper JL, Matthews JB, Besong AA, Stone MH, Ingham E (2001) A novel method for the prediction of functional biological activity of polyethylene wear debris. *Proc Inst Mech Eng H J Eng Med* 215(2):127–132. <https://doi.org/10.1243/0954411011533599>
81. Maxian TA, Brown TD, Pedersen DR, Callaghan JJ (1996) A sliding-distance-coupled finite element formulation for polyethylene wear in total hip arthroplasty. *J Biomech* 29(5):687–692. [https://doi.org/10.1016/0021-9290\(95\)00125-5](https://doi.org/10.1016/0021-9290(95)00125-5)

82. Teoh SH, Chan WH, Thampuran R (2002) An elasto-plastic finite element model for polyethylene wear in total hip arthroplasty. *J Biomech* 35:8
83. Buford A, Goswami T (2004) Review of wear mechanisms in hip implants: paper I – general. *Mater Des* 25(5):385–393. <https://doi.org/10.1016/j.matdes.2003.11.010>
84. Essner A, Schmidig G, Wang A (2005) The clinical relevance of hip joint simulator testing: in vitro and in vivo comparisons. *Wear* 259(7–12):882–886. <https://doi.org/10.1016/j.wear.2005.02.105>
85. Oral E, Christensen SD, Malhi AS, Wannomae KK, Muratoglu OK (2006) Wear resistance and mechanical properties of highly cross-linked, ultrahigh-molecular weight polyethylene doped with vitamin E. *J Arthroplast* 21(4):580–591. <https://doi.org/10.1016/j.arth.2005.07.009>
86. Kang L, Galvin AL, Brown TD, Jin Z, Fisher J (2008) Quantification of the effect of cross-shear on the wear of conventional and highly cross-linked UHMWPE. *J Biomech* 41(2):340–346. <https://doi.org/10.1016/j.jbiomech.2007.09.005>
87. Kang L, Galvin AL, Fisher J, Jin Z (2009) Enhanced computational prediction of polyethylene wear in hip joints by incorporating cross-shear and contact pressure in addition to load and sliding distance: effect of head diameter. *J Biomech* 42(7):912–918. <https://doi.org/10.1016/j.jbiomech.2009.01.005>
88. Jin ZM, Fisher J, Brown TD, Galvin AL, Kang L (2008) Wear simulation of ultra-high molecular weight polyethylene hip implants by incorporating the effects of cross-shear and contact pressure. *Proc Inst Mech Eng H J Eng Med* 222(7):1049–1064. <https://doi.org/10.1243/09544119jeim431>
89. Mattei L, Di Puccio F, Ciulli E (2013) A comparative study of wear laws for soft-on-hard hip implants using a mathematical wear model. *Tribol Int* 63:66–77. <https://doi.org/10.1016/j.triboint.2012.03.002>
90. Liu F, Fisher J, Jin Z (2012) Computational modelling of polyethylene wear and creep in total hip joint replacements: effect of the bearing clearance and diameter. *Proc Inst Mech Eng H J Eng Tribol* 226(6):552–563. <https://doi.org/10.1177/1350650112441908>